MIPAS Observations of Ozone in the Middle Atmosphere

Manuel López-Puertas[1], Maya García-Comas[1], Bernd Funke[1], Angela Gardini[1], Gabriele P. Stiller[2], Thomas von Clarmann[2], Norbert Glatthor[2], Alexandra Laeng[2], Martin Kaufmann[3], Viktoria F. Sofieva[4], Lucien Froidevaux[5], Kaley A. Walker[6], and Masato Shiotani[7]

[1]Instituto de Astrofísica de Andalucía, CSIC, Granada, Spain
[2]Karlsruhe Institute of Technology, Institute of Meteorology and Climate Research, Karlsruhe, Germany
[3]Institute for Energy and Climate Research, Research Centre Jülich, Jülich, Germany
[4]Finnish Meteorological Institute, Earth Observation, Helsinki Finland
[5]Jet Propulsion Laboratory, California Institute of Technology, Pasadena, CA, USA
[6]6 Department of Physics, University of Toronto, Toronto, Ontario, Canada
[7]Research Institute for Sustainable Humanosphere, Kyoto University, Uji, Kyoto, Japan

Correspondence to: M. López-Puertas (puertas@iaa.es)

Abstract. In this paper we describe the stratospheric and mesospheric ozone (version V5r_O3_m22) distributions retrieved from MIPAS observations in the three middle atmosphere modes (MA, NLC and UA) taken with an unapodized spectral resolution of $0.0625\,\mathrm{cm}^{-1}$ from 2005 until April 2012. O_3 is retrieved from microwindows in the $14.8\,\mu m$ and $10\,\mu m$ spectral regions and requires non-LTE modelling of the O_3 v_1 and v_3 vibrational levels. Ozone is reliably retrieved from 20 km in the MA mode (40 km for UA and NLC) up to $\sim 105\,\mathrm{km}$ during dark conditions and up to $\sim 95\,\mathrm{km}$ during illuminated conditions. Daytime MIPAS O_3 has an average vertical resolution of 3-4 km below 70 km, 6-8 km at 70–80 km, 8-10 km at 80–90 km and 5–7 km at the secondary maximum (90–100 km). For nighttime conditions the vertical resolution is similar below 70 km, and better in the upper mesosphere and lower thermosphere: 4-6 km at 70–100 km, 4–5 km at the secondary maximum, and 6–8 km at 100–105 km. The noise error for daytime conditions is typically smaller than 2% below 50 km, 2–10% between 50 and 70 km, 10-20% at 70-90 km and $\sim 30\%$ above 95 km. For nighttime, the noise errors are very similar below around 70 km but significantly smaller above, being 10-20% at 75-95 km, 20-30% at 95-100 km and larger than 30% above 100 km. The additional major O_3 errors are the spectroscopic data uncertainties below 50 km (10-12%), and the non-LTE and temperature errors above 70 km. The validation performed suggests that the spectroscopic errors below 50 km, mainly caused by the O_3 air-broadened half-widths of the v_2 band, are overestimated. The non-LTE error (including the uncertainty of atomic oxygen at nighttime) is relevant only above $\sim 85\,\mathrm{km}$ with values of 15–20%. The temperature error varies from $\sim 3\%$ up to 80 km to 15-20% near 100 km. Between 50 and 70 km, the pointing and spectroscopic errors are the dominant uncertainties. The validation performed in comparisons with SABER, GOMOS, MLS, SMILES and ACE-FTS shows that MIPAS O_3 has an accuracy better than 5% at and below 50 km, with a positive bias of a few percent. In the 50-75 km region, MIPAS O_3 has a positive bias of $\approx 10\%$, which is possibly caused in part by O_3 spectroscopic errors in the $10\,\mu m$ region. Between 75 and 90 km, MIPAS nighttime O_3 is in agreement with other instruments by 10%, but for daytime the agreement is slightly larger, ~ 10-20%. Above 90 km, MIPAS daytime O_3 is in agreement with other instruments by 10%. At nighttime, however, it shows a positive bias increasing from 10% at 90 km to 20% at 95-100 km, the latter of which is attributed to the large atomic oxygen

abundance used. We also present MIPAS O_3 distributions as function of altitude, latitude and time, showing the major O_3 features in the middle and upper mesosphere. In addition to the rapid diurnal variation due to photochemistry, the data also show apparent signatures of the diurnal migrating tide, both during day and nighttime, as well as the effects of the semi-annual oscillation above $\sim$70 km in the tropics and mid-latitudes. The tropical daytime O_3 at 90 km shows a solar signature in phase

5   with the solar cycle.

1   Introduction

Ozone is a key constituent of the atmosphere playing a major role in its energy budget and chemistry, particularly in the stratosphere and upper mesosphere (Brasseur and Solomon, 2005). Typical ozone profiles show two clearly distinguished maxima, one located between 10 and 35 km, the so-called ozone layer, where most ozone resides, and a secondary maximum

10   around the mesopause ($\sim$90-95 km). Ozone has been extensively measured in the stratosphere and also in the mesosphere using different techniques (see, e.g. Kaufmann et al. (2003) for measurements taken prior to 2003 and Smith et al. (2013) for the most recent observations, mainly from satellite instruments). Measurements that cover the atmosphere from the lower stratosphere up to the lower thermosphere, both at day- and night-time conditions and with global latitudinal coverage are, however, not very frequent. MIPAS (Michelson Interferometer for Passive Atmospheric Sounding) is a high-resolution limb

15   sounder on board the Envisat satellite, launched on March 1, 2002 and taking measurements until 8 April 2012, when the Envisat satellite failed. The satellite was inserted into a polar sun-synchronous orbit at an inclination of 81.5° and altitude of about 800 km. The orbital period was about 101 min, achieving a global coverage of the Earth with 14.3 daily orbits, with the descending (North to South) part crossing the Equator at approximately 10:00 local time (LT) and the ascending part crossing it at approximately 22:00 LT (hereafter called as am and pm measurements). MIPAS had a wide spectral coverage and a

20   high spectral resolution, operating at 0.025 cm^{-1} during 2002-2004 and 0.0625 cm^{-1} from 2005 until the 8th of April 2012 (Fischer et al., 2008). MIPAS operated with a global latitude coverage (pole-to-pole) and performed measurements during day and night. The instrument spent most of the time observing in the 6-68 km altitude range (the nominal mode, NOM) but it also regularly looked at higher altitudes in its middle atmosphere (MA), noctilucent (NLC), and upper atmosphere (UA) modes (De Laurentis, 2005; Oelhaf, 2008). The retrieval of ozone from the NOM mode has been carried out, among others, by the

25   Institute of Meteorology and Climate Research and Instituto de Astrofísica de Andalucía (IMK/IAA) (Glatthor et al., 2006). In that inversion local thermodynamic equilibrium (LTE) is assumed, which is a good approximation up to about 50 km and a reasonable approach up to about 60 km (von Clarmann et al., 2009). MIPAS took a few spectra of the middle atmosphere (only half a day of measurements on 11 June 2003) with its full spectral resolution mode. Ozone concentrations were retrieved from those spectra from the low stratosphere up to the lower thermosphere including the non-LTE effects (Gil-López et al., 2005). In

30   this paper we focus on the inversion of ozone from the bulk of MIPAS observations of the middle atmosphere taken from 2005 until April 2012 in three different modes (MA, NLC and UA) with the optimized spectral resolution of 0.0625 cm^{-1}. Part of this dataset (2008-2009), version V4O_O3_m02, was previously retrieved and used in some studies (e.g., Smith et al., 2013). Here we describe the inversion of the entire MA/UA/NLC period, 2005-2012, version V5r_O3_m22, derived from V5 L1b

spectra. The method is essentially described in Gil-López et al. (2005). Here we review several aspects of the retrieval baseline including the changes in the non-LTE modeling of O_3 and the new microwindows (MWs) used. In addition, an assessment of the quality of the middle atmosphere O_3 data, a comparison with the previous version V4O_O3_m02 (sometimes referred to as V4O_502), and a validation with recent middle atmosphere ozone measurements taken by SABER, GOMOS, MLS, SMILES and ACE-FTS, are also presented. Finally we describe the major features of the O_3 database focusing on the mesosphere.

2 O_3 non-LTE modelling

As mentioned below most of the microwindows used in the retrieval of O_3 in the mesosphere are located in the $9.6\,\mu\text{m}$ region, where the v_1 and v_3 fundamental, combinational and hot bands arise. We discuss here the non-LTE modelling of those vibrational levels. The v_2 fundamental band is used only at the lower altitudes, below $50\,\text{km}$, where it is in LTE (Funke et al., 2012). We should clarify that the non-LTE populations of O_3 used in the retrieval have been calculated with the Generic RAdiative traNsfer AnD non-LTE population algorithm (GRANADA) (see Sec. 3). In this section we describe a simplified formulation of non-LTE for O_3 with the aim of showing the quantities required for performing the retrieval.

The major processes affecting the populations of the vibrationally excited $O_3(v_1,v_2,v_3)$ levels are discussed in detail by López-Puertas and Taylor (2001) and are listed in Table 1. The collisional processes (1-4) have been adapted from Table 7 in Funke et al. (2012), to which we have added the simplified radiative processes of a) the absorption of radiation from the layers below (process 5) and b) the spontaneous emission (process 6).

Table 1. Collisional and radiative processes affecting the O_3 vibrational levels.

No.	Rate	Process
1	k_1	$O_2 + O + M \rightarrow O_3(v_1,v_2,v_3)$
2	$k_{vt,M}$	$O_3(v_1,v_2,v_3) + M \rightleftharpoons O_3(v'_1,v'_2,v'_3) + M$
3	k_{chem}	$O_3(v_1,v_2,v_3) + O \rightarrow O_2 + O_2$
4	$k_{vt,O}$	$O_3(v_1,v_2,v_3) + O \rightarrow O_3(v'_1,v'_2,v'_3) + O$
5	J_{Earth}	$O_3 + h\nu \rightarrow O_3(v_1,v_2,v_3)$
6	A	$O_3(v_1,v_2,v_3) \rightarrow O_3(v'_1,v'_2,v'_3) + h\nu$

Note that the energy of the $O_3(v_1,v_2,v_3)$ level is larger than that of $O_3(v'_1,v'_2,v'_3)$.

From the statistical equilibrium assumption and the processes listed in Table 1 the population of the vibrationally excited $O_3(v_3)$ levels (we focus here on v_3, from whose emission we are retrieving O_3) can be obtained, approximately, by

$$\frac{[O_3(v_3)]}{[O_3]} = \frac{J_{Earth} + p_t + p_{nt}}{A + k_{vt,M}[M] + k_{vt,O}[O] + k_{chem}[O]}, \tag{1}$$

where the brackets denote concentrations, J_{Earth} is the excitation rate of $O_3(v_3)$ due to the absorption of ν_3 photons coming from the lower atmospheric regions (upwelling flux), A is the Einstein coefficient of the $\nu_3 = 1$ band, [O] the atomic oxygen

concentration, [M] the air molecules concentration (sum of N_2 and O_2) and the other collisional rates are defined in Table 1. p_t is the specific thermal production of $O_3(v_3)$ given by

$$p_t = k_{vt,M}[\text{M}] \exp[-E(v_3)/kT], \tag{2}$$

where T is the kinetic temperature, k the Boltzmann constant and $E(v_3)$ the energy of the $O_3(v_3)$ level. The specific production due to non-thermal processes (chemiluminescence, process 1 in Table 1), p_{nt}, is given by

$$p_{nt} = k_1 [\text{O}_2] [\text{M}] ([\text{O}]/[\text{O}_3]) \, \phi(v_3), \tag{3}$$

where $\phi(v_3)$ is the fraction of the O_3 molecules produced by process 1 which finally end excited in the $O_3(v_3)$ level. In practice, $\phi(v_3)$ depends not only on the nascent distribution of reaction 1 but also, and mainly for the lower v_3 levels, on the radiative and collisional relaxations of the more energetic (v_1,v_2,v_3) levels, that is on $A, k_{vt,M}, k_{vt,O}$ and k_{chem} for those levels and also on [M] and [O]. From all those parameters, the only unknown in our case is the atomic oxygen concentration, [O].

For the retrieval of O_3, one would like the $[O_3(v_3)]/[O_3]$ ratio of Eq. 1, which is proportional to the $O_3(v_3)$ vibrational temperature and hence to the measured O_3 emission, to be the least dependent as possible on kinetic rates and other atmospheric parameters. For the MIPAS O_3 retrieval, all the parameters in Eqs. 1, 2 and 3 are known, or measured simultaneously by MIPAS, except [O].

Table 2. Major photochemical reactions affecting O_3 in the mesosphere and lower thermosphere.

No.	Rate	Process
1	k_1	$O_2 + O + M \rightarrow O_3(v_1,v_2,v_3)$
2	k_2	$H + O_3 \rightarrow OH^*(v) + O_2$
3	k_3	$O + O_3 \rightarrow O_2 + O_2$
4	J_{Sun}	$O_3 + h\nu \rightarrow O_2 + O$

Because of the rapid timescales for ozone production and loss in the non-LTE region, the assumption of photochemical equilibrium above around 60 km is valid. Thus, from the major photochemical reactions affecting O_3 in the mesosphere and lower thermosphere (see Table 2), the non-thermal production, p_{nt}, and [O] are given for daytime conditions, respectively, by

$$p_{nt,day} = J_{Sun} \, \phi(v_3) \quad \text{and} \tag{4}$$

$$[\text{O}]_{\text{day}} \approx \frac{J_{Sun} [\text{O}_3]}{k_1 [\text{O}_2] [\text{M}]}, \tag{5}$$

where the chemical losses (k_2 and k_3) have been neglected. In this way, we have no major limitation of unknown atmospheric parameters in the O_3 non-LTE retrieval during daytime if we update the non-LTE model with the O_3 abundance in each iteration.

During nighttime, assuming also photochemical equilibrium and the processes in Table 2, the non-thermal production and [O] are given, respectively, by

$$p_{nt,night} = \frac{k_2[\text{H}]}{1 - \frac{k_3[\text{O}_3]}{k_1[\text{O}_2][\text{M}]}} \quad \text{and} \tag{6}$$

$$[\text{O}]_{\text{night}} \approx \frac{k_2[\text{H}][\text{O}_3]}{k_1[\text{O}_2][\text{M}] - k_3[\text{O}_3]}. \tag{7}$$

In this case, even iterating, we still have the unknown of the atomic hydrogen concentration, [H], which has to be taken from models or from parameterization. As we see, the non-thermal production at nighttime is directly proportional to [H]. Then, in order to estimate the errors introduced by the uncertainty in [H], it is worthwhile to estimate how important is the contribution of the non-thermal term, $p_{nt,night}$ in Eq. 6, in comparison with the radiative and thermal contributions, J_{Earth} and p_t in Eq. 1. Figure 1 show the calculations of these terms computed with the GRANADA model for a few nighttime profiles for two days typical of equinox and solstice. The figure shows that the contribution of the non-thermal term to the excitation of $O_3(v_3=1)$ is, in the worst case, a factor of 5 smaller than the radiative and thermal excitations. We then expect that the uncertainties in the inputed [H] from the NRLMSIS-00 model (Picone et al., 2002, see below) would not introduce large uncertainties in the retrieved O_3. This effect, however, is larger for higher O_3 vibrational levels because for these states the radiative term is negligible and the non-thermal part is larger. Thus the uncertainty in [H] might introduce a larger error for the case of wide band radiometers measuring a significant contribution of the hot bands emission.

3   Ozone non-LTE retrieval

As described above, we used MIPAS spectra taken in the MA, NLC, and UA modes. In the MA mode, the spectra are taken at limb tangent heights from about 20 km up to 102 km with a vertical spacing of 3 km. The UA mode ranges from about 42 km up to 172 km, which has a 3 km vertical sampling up to 102 km and 5 km above. The NLC mode is a variant of the MA mode specifically tailored for measuring the NLCs during the summers (De Laurentis, 2005; Oelhaf, 2008). In this mode the spectra are taken at tangent heights from 39 km up to 78 km at 3-km steps; from 78 km up to 87 km at 1.5 km steps, and from 87 km up to 102 km again in 3-km steps. MIPAS horizontal field of view (FOV) is approximately 30 km.

The method used for the inversion of ozone under non-LTE conditions is essentially described in Gil-López et al. (2005). In that work the retrieval was adapted for the very few (only 26 orbits) MIPAS data of the upper atmosphere taken on June 2003 at the full spectral resolution of 0.025 cm^{-1}. Here we briefly summarize the approach, discuss the new MWs used in the inversion of the MA, NLC and UA observational modes (taken at 0.0625 cm^{-1}), and review the changes in the non-LTE modeling of O_3 vibrational levels.

The MIPAS V5r_O3_m22 ozone retrieval is based on a constrained multilinear least squares fitting of non-LTE limb radiances. That is performed using the IMK/IAA Scientific Processor (von Clarmann et al., 2003, 2009) extended with the non-LTE GRANADA algorithm (Funke et al., 2012), which is able to cope with non-LTE emissions. Funke et al. (2001) describe the peculiarities of the retrievals under consideration of non-LTE. The basic retrieval equations, the methods for characterization
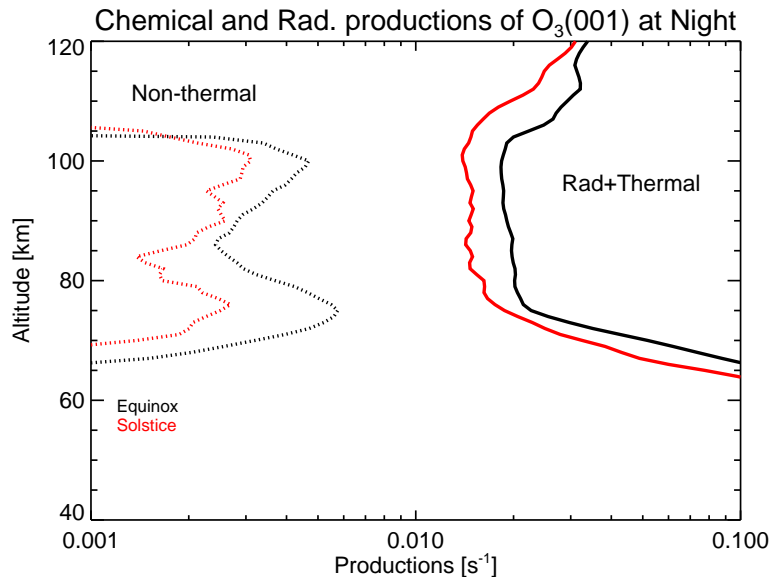
Figure 1. Specific production terms of the population of $O_3(001)$ at nighttime for two days typical of equinox (black) and solstice (red). Dotted lines are the specific non-thermal productions of $O_3(v_3=1)$ (Eq. 6), and solid lines are the sum of the radiative absorption and thermal collisions, J_{Earth} and p_t in Eq. 1.

of results through error estimates and vertical and horizontal averaging kernels, the iteration and convergence criteria and the regularization method are described in von Clarmann et al. (2003, 2009). Version V5 (5.02/5.06) of the ESA-calibrated L1b spectra was used (see Raspollini et al., 2010, and references therein).

The inversion is performed after a retrieval of the residual spectral shift and the non-LTE retrieval of temperature (García-Comas et al., 2012; García-Comas et al., 2014). The IMK/IAA processor simultaneously retrieves, besides the O_3 abundance, microwindow- and altitude-dependent continuum radiation and zero level calibration corrections (the latter, assumed constant with altitude).

The retrievals are performed from the surface to 120 km over a fixed altitude grid of 1 km up to 50 km, at 72-75 km, and at 77-88 km; of 2 km at 50-72 km, 75-77 km, and 88-102 km; and of 5 km from 105 up to 120 km. The grids have been selected as a trade-off between higher accuracy and computational efficiency. The forward calculations are performed using the same grid. The over-sampled retrieval grid, finer than the MIPAS vertical sampling of 3 km, makes necessary the use of a regularization in order to obtain stable solutions. We used here a Tikhonov-type first order smoothing constraint (Tikhonov, 1963). The numerical integration of the signal over the 3 km FOV is done using five pencil beams. The selected width of the integration window (apodized instrument line shape function) avoids channel border effects. Forward model calculations along the line of sight (LOS) are done considering horizontal gradient corrections. Thus, they account for changes in the populations (either in LTE or in non-LTE) of the emitting O_3 levels along the LOS due to kinetic temperature variations.

Table 3. Microwindows and altitude ranges used in the retrieval of MIPAS ozone V5r_O3_m22.

No.	Wavenumber (cm^{-1}) Minimum	Maximum	Altitudes (km)
1	687.6875	688.6875	
2	689.3125	691.8750	
3	692.2500	695.1875	
4	707.1250	710.0625	
5	712.3125	713.4375	
6	713.5000	716.4375	
7	716.5000	719.4375	
8	720.7500	723.6875	
9	728.5000	729.3750	
10	730.0625	730.5000	
11	731.9375	732.8750	
12	734.0000	734.7500	
13	736.4375	739.3750	
14	739.4375	741.9375	
15	745.2500	745.6875	
16	746.6875	747.1250	
17	747.6250	748.3750	
18	749.5625	752.5000	
19	752.9375	755.8750	
20	758.3750	759.4375	
21	759.5000	761.8750	
22	765.0000	765.6250	
23	767.5000	768.0000	
24	771.8750	772.1250	
25	774.2500	774.5625	
26	776.5000	776.7500	
27	780.2500	781.9375	
28	788.9375	789.6875	
29	790.7500	791.0000	
30	791.1875	791.5625	
31	1034.1250	1034.3750	
32	1034.4375	1035.0000	
33	1038.1875	1039.0000	
34	1040.0000	1040.8125	
35	1048.8125	1049.5000	
36	1050.6250	1051.8125	
37	1053.3125	1053.8125	
38	1054.6875	1055.5000	

Altitude column headers (km): 18, 21, 24, 27, 30, 33, 36, 39, 42, 45, 48, 51, 54, 57, 60, 63, 66, 69, 72, 75, 78–102

Ozone is reliably retrieved from 20 km in the MA mode (40 km for the UA and NLC modes) up to ∼105 km during dark conditions and up to ∼95 km during illuminated conditions. The logarithm of the volume mixing ratio (vmr) is retrieved from MWs covering ro-vibrational emissions of the O_3 main isotope. They have been selected from a broad spectral region, covered by channel A (685–970 cm^{-1}), and channel AB (1020–1170 cm^{-1}), and they vary with tangent altitudes in order to optimize computation time and minimize systematic errors (von Clarmann and Echle, 1998). The MWs used are listed in Table 3, and Fig. 2 shows some examples of single MIPAS spectra in the A and AB channels. The microwindows are an extension of the set used for the ozone retrieved from the MIPAS NOM mode of observation, covering altitudes below 70 km (von Clarmann et al., 2009). Below 50 km, we use the same MWs as in the NOM retrieval, located all in channel A. Above 50 km, the MWs used are mainly located in channel AB and are strongly affected by non-LTE.
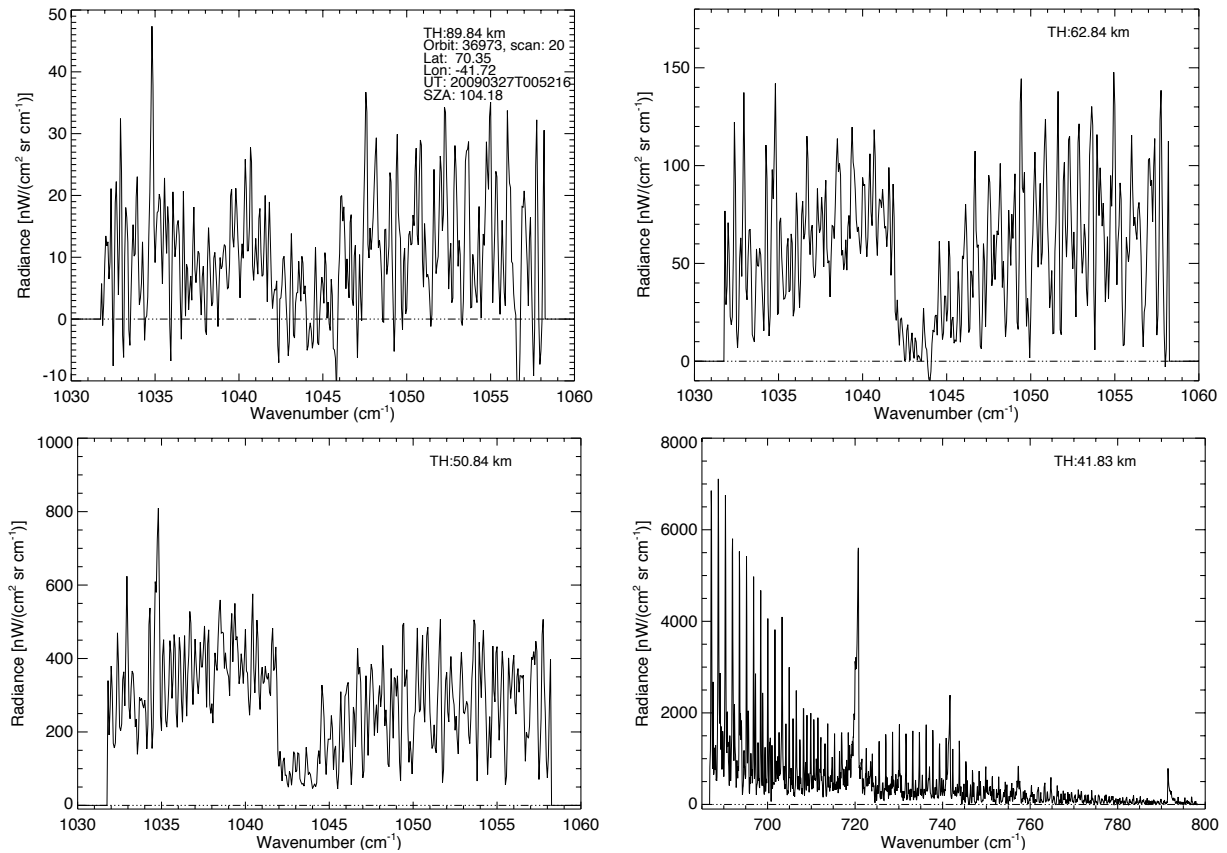
Figure 2. Examples of MIPAS L1b apodized single spectra in channels A (bottom/right panel) and in channel AB (rest of panels) at several tangent heights (as labeled) used in the inversion of O_3. The geolocation of the spectra is given in the top/left panel. The radiance in the 1030-1060 cm^1 spectral region is dominated by O_3 features. However, in channel A (bottom/right), it is dominated by CO_2 emissions and the O_3 contribution is hardly noticed.

The MIPAS V5r_O3_m22 ozone retrieval setup uses the following inputs. The O_3 a priori is taken from a MIPAS dedicated climatology (similar to that described in Funke et al., 2012). Pressure, LOS, temperature, and temperature horizontal gradients are taken from MIPAS T-LOS retrieval V5r_T_m21 (García-Comas et al., 2014). They have been retrieved from the CO_2 emission near 15 μm, recorded in channel A, and accounting for the non-LTE effects. The detailed description of the method and the characterization of the inverted pressure-temperatures profiles are described in García-Comas et al. (2012). The upgrades in the retrieval of the temperature used here (V5r_T_m21) and a validation of the results are reported by García-Comas et al. (2014). This version of MIPAS temperatures correct the main systematic errors of the previous version and have, in general, a remarkable agreement with the measurements taken by ACE-FTS, MLS, OSIRIS, SABER, SOFIE and the Rayleigh lidars at Mauna Loa and Table Mountain. In the region of interest here, however, there are still significant differences, with the MIPAS mesopause differing by 5-10 K from the other instruments, being warmer than SABER, MLS and OSIRIS and colder than ACE-FTS and SOFIE.

The O_3 spectroscopic data were taken from the HITRAN 2008 database (Rothman et al., 2009). A test performed using the HITRAN 2016 O_3 database (Gordon et al., 2017) has shown that the radiances are just marginally larger (only 0.5% in channel A and 0.25% in channel AB).

The O_3 non-LTE vibrational populations were computed online in each iteration of the inversion by using the GRANADA model (Funke et al., 2012). As described above, the O_3 non-LTE model requires several inputs. The set of O_3 vibrational levels, the non-LTE collisional scheme and the rate constants are based on the GRANADA model except as noted below.

The exponent a in the rate $k_1 = 6.0 \times 10^{-34}\,(T/300)^a$ of reaction $O + O_2 + M \rightarrow O_3(v_1, v_2, v_3) + M$ has been updated from 2.3 to 2.4 following Burkholder et al. (2015). This has a small effect on the O_3 v_1 and v_3 vibrational temperatures and also on the retrieved O_3.

The collisional deactivation of $O_3(v_1, v_2, v_3)$ (process 2 in Table 1) with Δv_1 or $\Delta v_3 = -1$ and $\Delta v_2 = 1$ (process 2c, k_d, in Table 7 of Funke et al. (2012)) was erroneously implemented in the previous version with a rate of $3.1 \times 10^{-15}\,(T/300)^{1/2}$. Now we include the expression in Table 7 of Funke et al. (2012) but limited to a minimum value of 4×10^{-16} cm^{3}s^{-1} at temperatures below 200 K (Menard et al., 1992). Although this change in the rate coefficient is rather large, its impact on the $O_3(v_3)$ vibrational temperature is very small, as it is dominated by the relaxation to v_2. This leads to an O_3 vmr about 5% smaller between 70 and 85 km.

The chemical quenching of vibrationally excited O_3 by O, $O_3(v_1, v_2, v_3) + O \rightarrow O_2 + O_2$, has been neglected in this version. This implies larger $O_3(v_3)$ vibrational temperatures and hence smaller retrieved O_3 abundances. Note, however, that the total quenching of $O_3(v_1, v_3)$ by O, including also collisional relaxation by O, process 4 in Table 1, is still within the measurement errors of the deactivation of $O_3(v_1, v_3)$ (West et al., 1976, 1978, see discussion below).

As shown in Sec. 2, the inversion of O_3 under non-LTE conditions requires knowledge of the atomic oxygen concentration, O. In our retrievals, we constrain the O abundance by employing photochemical equilibrium with the O_3 abundance retrieved in the previous iteration. This photochemical constraint for [O]/[O_3] is an optional feature in GRANADA which has been switched on in this retrieval below 97 km.

At nighttime, the non-thermal production and O depends not only on O_3 but also on hydrogen, H (see Eqs. 6 and 7). For this reason, we use the H abundance from the NRLMSIS-00 model (Picone et al., 2002) in the photochemical equilibrium computation. Above 97 km we use the atomic oxygen from the Whole Atmosphere Community Climate Model with specified dynamics (SD-WACCM) simulations spanning over the time period of the measurements (Garcia et al., 2014). To be more precise both profiles were merged in the 92-102 km region using a hyperbolic tangent function centred at 97 km. SD-WACCM (in the following just WACCM) is constrained with output from NASA's Modern-Era Retrospective Analysis (MERRA) (Rienecker et al., 2011) below approximately 1 hPa. The main reason for including WACCM about that altitude is motivated by the lack or incorrect latitudinal and seasonal variation of atomic oxygen in the NRLMSIS-00 model.

The forward model also includes the contribution (as a potential overlap with O_3 lines) of CO_2 lines. As for O_3, we also include the emissions by CO_2 bands in non-LTE. A detailed description of the CO_2 non-LTE model used and all the required input parameters can be found in Jurado-Navarro et al. (2016).
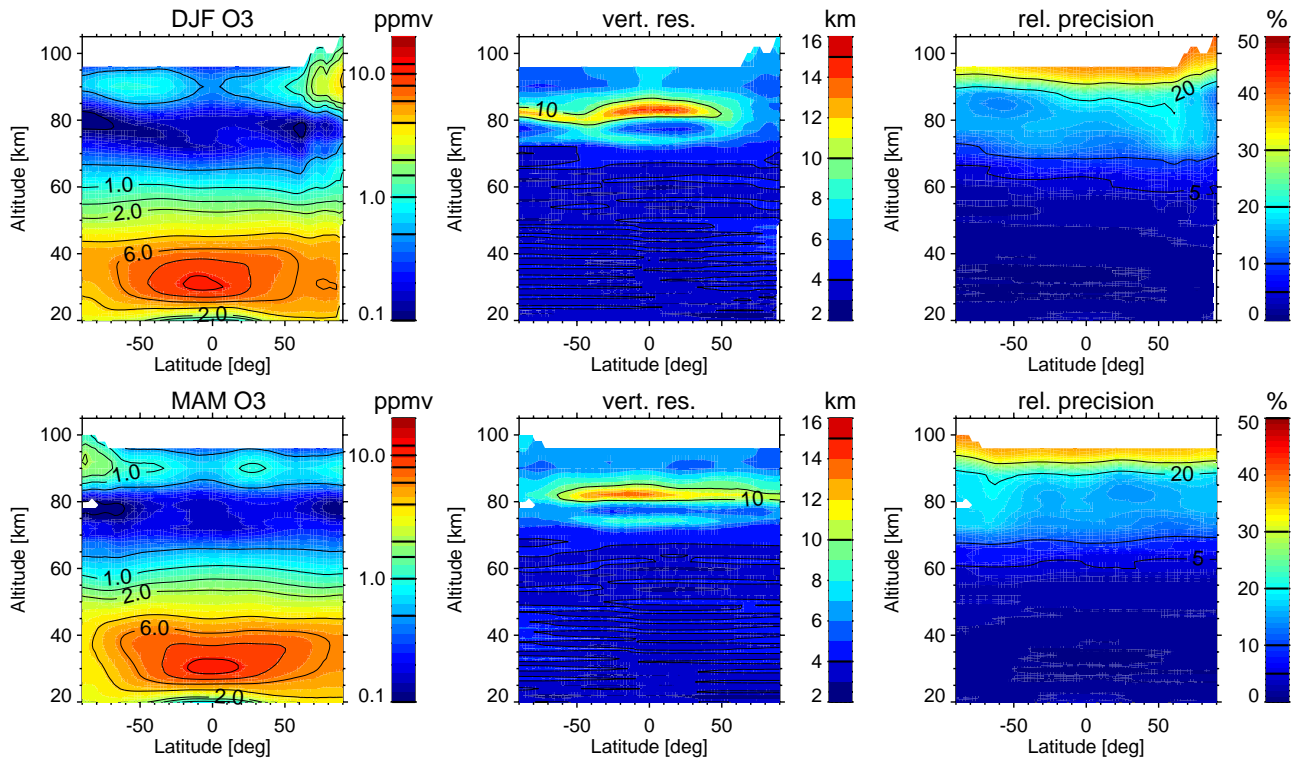
Figure 3. Latitude-altitude cross sections of MIPAS MA daytime ozone (left), its vertical resolution (center) and single profile noise error (1σ, right) for solstice (December-January-February: DJF) (top row) and equinox (March-April-May; MAM) (bottom row). All measurements from 2005 to 2012 are included. White areas denote regions where the retrieved O_3 is not significant. Contour lines are marked in the color bar scale.

4   Characterization of the retrieved O_3 and error analysis

Figures 3 and 4 show seasonal zonal means of O_3 retrieved from MIPAS and the mean of the noise error (1σ) and vertical resolution for the middle atmosphere (MA) mode for daytime (10 am) and nighttime (10 pm) conditions, respectively. The results for the UA and NLC modes are very similar except that the O_3 is retrieved above 40 km instead of 20 km. The ozone
5   fields are included in these figures only for a reference to the noise and vertical resolution; its major features and the vertical and latitude distributions are discussed in Sec. 7 below. Two seasons are shown; the noise error and vertical resolution for the other two seasons are very similar.

The vertical resolution of the MIPAS retrieved ozone is given by the full width at half maximum of the averaging kernels rows. For daytime, the O_3 average vertical resolution is 3-4 km below 70 km, 6-8 km at 70–80 km, 8-10 km at 80–90 km
10   (although it can be coarser in tropical regions), and 5–7 km at the secondary maximum (90–100 km). For nighttime conditions the vertical resolution is similar below 70 km, and it is better in the upper mesosphere and lower thermosphere. It is 4-6 km at 70–100 km (except a narrow region near 80 km where it takes values of 8-10 km), 4–5 km at the secondary maximum; and 6–8 km at 100–105 km.
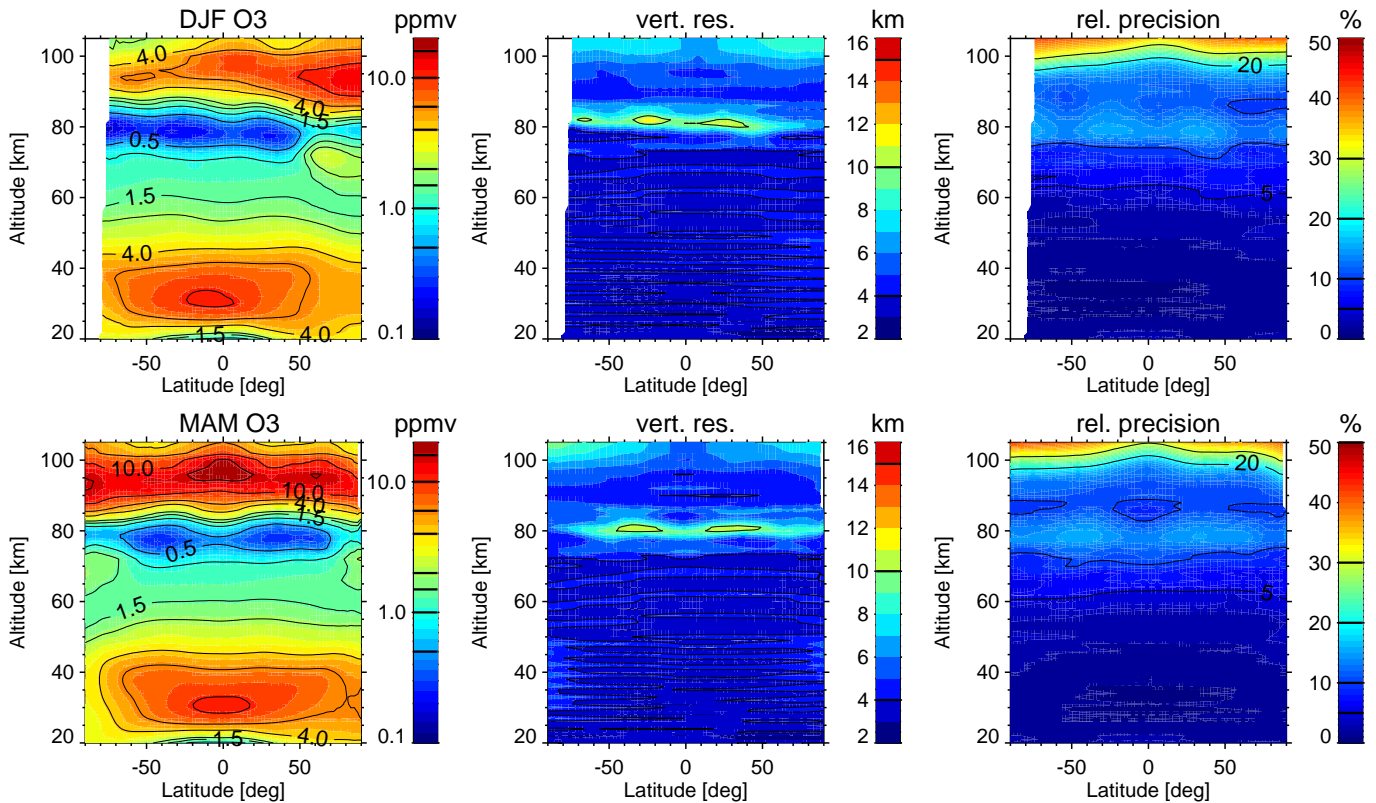
Figure 4. As Fig. 3 but for nighttime conditions.

Two criteria are recommended to be used to screen the retrieved O$_3$ version V5r_O3_m22 data in order to guarantee the quality of the profiles: a) the retrieved O$_3$ values of individual profiles where the diagonal value (or the mean diagonal value when averaging) of the averaging kernel is less (in absolute value) than 0.03 are considered non-trustful, and b) those values corresponding to altitudes not sounded by MIPAS (below the lowermost tangent altitude) and flagged by the visibility flag should not be used.

The error budget described here considers the propagation of the measurement noise and of the uncertainties of model parameters onto the retrieved ozone abundances. Noise-induced retrieval errors (as well as the vertical resolution, see above) are estimated routinely for each individual profile by the retrieval algorithm. The ozone noise error is calculated assuming a wavelength-dependent noise-equivalent-spectral-radiance which has approximated average values of 17 and 10 nW/(cm^{2}cm^{-1}sr) for channels A and AB, respectively. Typical values (1σ) for daytime (see the right column of Fig. 3) are smaller than 2% below 50 km, 2-10% between 50 and 70 km, 10-20% at 70-90 km and about 30% above 95 km. For nighttime (see right column of Fig. 4), the noise errors are very similar below around 70 km but significantly smaller above, being 10-20% at 75-95 km, 20-30% at 95-100 km and larger than 30% above 100 km.
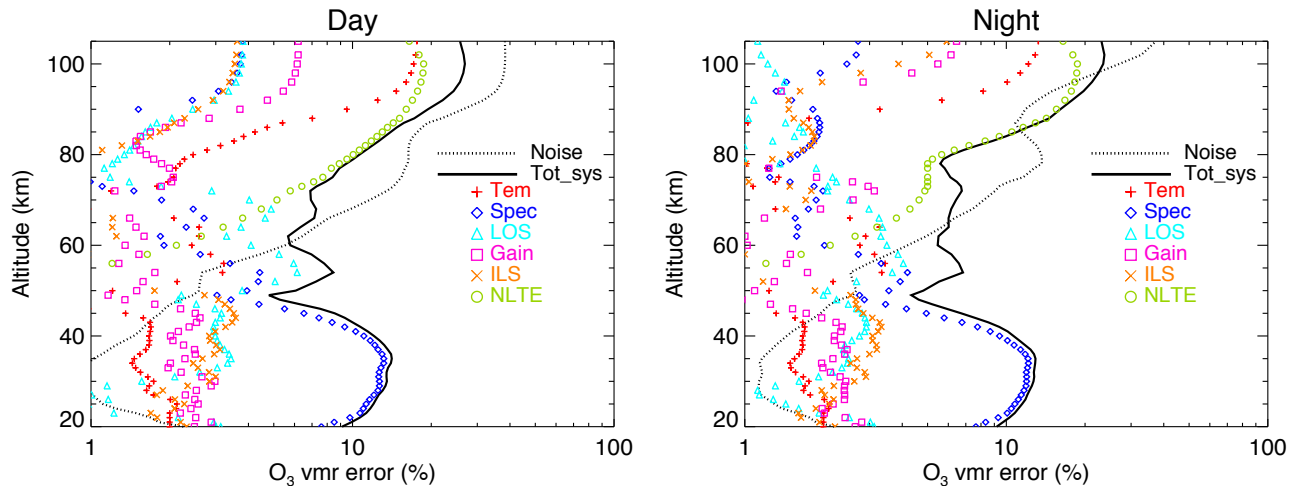
Figure 5. Errors of the retrieved O_3 vmr for daytime (left) and nighttime (right) in relative values. The different sources are described in the legend of Table 4.

Table 4. Summary of main errors (1σ) of ozone vmr in %. Errors refer to nighttime conditions with daytime values, when different, in parentheses. 'NLTE' includes errors due to uncertainties in the collisional rates of the non-LTE model and in the atomic oxygen (see text). 'Total (Syst.)' is the root sum square of all systematic errors (noise is not included). LOS stands for Line Of Sight, 'Tem' for temperature, ILS for Instrument Line of Shape, and 'Spec.' for spectroscopy.

Height (km)	Noise	LOS	Gain	Tem	ILS	Spec.	NLTE	Total (Syst.)
100	27 (38)	1.2 (3.8)	5.5 (6.2)	12 (17)	4.0	2.5 (3.7)	19	24 (27)
95	17 (36)	1.4 (3.5)	2.1 (5.6)	9 (15)	1.8 (3.3)	1.4 (3.3)	18	21 (25)
90	12 (26)	1.0 (2.5)	0.32 (3.7)	3.3 (9.5)	1.5 (2.6)	1.8	16	16 (19)
80	14 (15-20)	0.8 (1.3)	0.34 (1.6)	0.8 (2.5)	1.5 (0.9)	1.6 (0.6)	6 (10)	6 (11)
70	8.2 (12)	2.5 (4)	2.6 (0.9)	0.4 (0.7)	1.7 (0.7)	1.9	5	6.4 (6.8)
60	4.2 (5.5)	3.5 (4.1)	1.0 (1.4)	2.8 (2.4)	0.7 (0.9)	2.0	2.0	5.5 (5.7)
50	2.7	2.1 (3.8)	1.1 (1.5)	1.2	1.9	3.6 (4)	0	4.8 (6)
40	1.5	2.7	2.2	1.7	3.1	9.4 (11)	0	11 (12)
30	1.1	1.6	2.4	1.8	2.6	12	0	13
20	2.2	3.1	2.6	2.0	2.2	7.6	0	9

Errors related to the mapping of uncertain model parameters on the retrieved ozone vmr are estimated for representative profiles for daytime and nighttime conditions. We name these "systematic" errors to distinguish them from the noise error, although they are not purely systematic but in some cases they also have a random component. We have calculated them by comparing the retrieved profiles obtained with the nominal parameter and with the perturbed parameter. Fig. 5 shows those errors (1σ), including also mean profiles of the noise errors shown in Figs. 3 and 4, and Table 4 lists them. The uncertainties assumed for the estimation of the systematic errors are 1% for gain calibration and 3% for the instrument line shape (ILS). For the elevation pointing (LOS) we have assumed an error of 150 m below 60 km, where we have information on the relative pointing from the temperature-LOS retrieval (von Clarmann et al., 2009; García-Comas et al., 2012). Above that height, where we obtain the LOS information from the engineering tangent altitudes of MIPAS (adjusted with the LOS retrieved below), we

assumed an error of 300 m. For temperature, the errors have been considered as 0.5 K below 50 km, 1 K at 50-70 km, 2 K at 70-80 km, 5 K at 80-100 km and 10 K above (García-Comas et al., 2014).

The spectroscopic errors have been estimated by J.-M. Flaud (personal communication, 2008). The errors assumed for the line intensities of the fundamental v_1, v_2 and v_3 bands (those mainly used here) are 2% for the strongest lines, 5% for the moderate lines, and 10% for the weaker lines. For the lines of the hot bands having as lower state (010), (020), (100) or (001), the error is in the range of 4-25%, increasing as the line intensity decreases. The errors considered for the more excited hot bands are larger, up to 30%, but their contributions to the selected MWs is small. The error assumed for the O_3 air-broadened half-widths is 12%. The larger O_3 spectroscopic errors below 50 km (see Fig. 5) are mainly due to the error in the half-widths. The contribution of the error in the line intensities is of only 2–3%.

The modelling of the non-LTE populations of the O_3 vibrational levels emitting near 9.6 μm is an important source of the MIPAS ozone systematic error above the mid-mesosphere. Non-LTE errors are dominated by the uncertainties in the collisional rates used in the non-LTE model. The three major sources are: 1) The error in the three-body reaction rate of O_3 formation; 2) the thermal relaxation of the $O_3(v_1,v_3)$ levels with N_2 and O_2; and 3) the collisional relaxation and/or chemical reaction of $O_3(v_1,v_3)$ levels with atomic oxygen. According to the current literature, we have considered uncertainties of 10% for the first, 20% for the second, and 50% for the third. For the later, West et al. (1976) derived experimentally the deactivation rate of $O_3(v_1,v_3)$ by O, and provided rates for both the thermal relaxation, $O_3(v_1,v_3) + O \rightarrow O_3 + O$, and the chemical reaction, $O_3(v_1,v_3) + O \rightarrow 2\,O_2$, assuming each one alone was responsible for the total deactivation. These authors could not estimate the relative contribution of each process and the error associated with these two rates is about 50%. West et al. (1978) further reported that the deactivation is most likely to occur through the thermal relaxation. Hence, we have considered that the deactivation takes place through the thermal relaxation (process 2 in Table 1) and assumed the measured error of West et al. (1976) of 50%.

We have not considered additional errors due to the uncertainty in the atomic oxygen (daytime) or atomic hydrogen (nighttime) below 95 km (the error due to the O_3 error itself is already taken into account). During daytime, this is reasonable because atomic oxygen is derived from the photochemical equilibrium with the retrieved O_3. At night, however, when the retrieval depends on the atomic hydrogen concentration, if the error in H is significantly smaller than the 50% assumed for the deactivation of $O_3(v_1,v_3)$, its contribution will not be significant. If comparable, however, we might be underestimating the non-LTE errors. Above 97 km, we have assumed an uncertainty in the WACCM atomic oxygen of 50%, leading to an error of about 10% in the retrieved O_3 in that region (see Fig. 6). This error has been added, quadratically, to the other components of the non-LTE uncertainties discussed above.

The uncertainty of the first of those three processes on O_3 is only important above $\sim$85 km, reaching a maximum of 5% in the retrieved O_3. The second one is significant only from $\sim$60 km up to $\sim$80 km, introducing an error of 2–5% in ozone for nighttime, and of 2–10% for daytime, including polar summer, where it might be slightly larger near 80 km. The third one, including the error in the atomic oxygen, is only significant above $\sim$85 km but it is the largest, with an estimated error in O_3 of 15–20% at 85-100 km. Overall, the non-LTE errors are typically negligible below 60 km, 2-10% at 60-80 km, and 15–20% above 85 km.

The overall systematic component of the O$_3$ abundance error is dominated by the spectroscopic data uncertainty below 50 km and by the non-LTE and temperature errors above about 70 km. Between 50 and 70 km, the pointing (LOS) and the spectroscopic errors are the dominant uncertainties. Our validation studies suggests, however, that the spectroscopic errors below 50 km are overestimated (see Sec. 6).
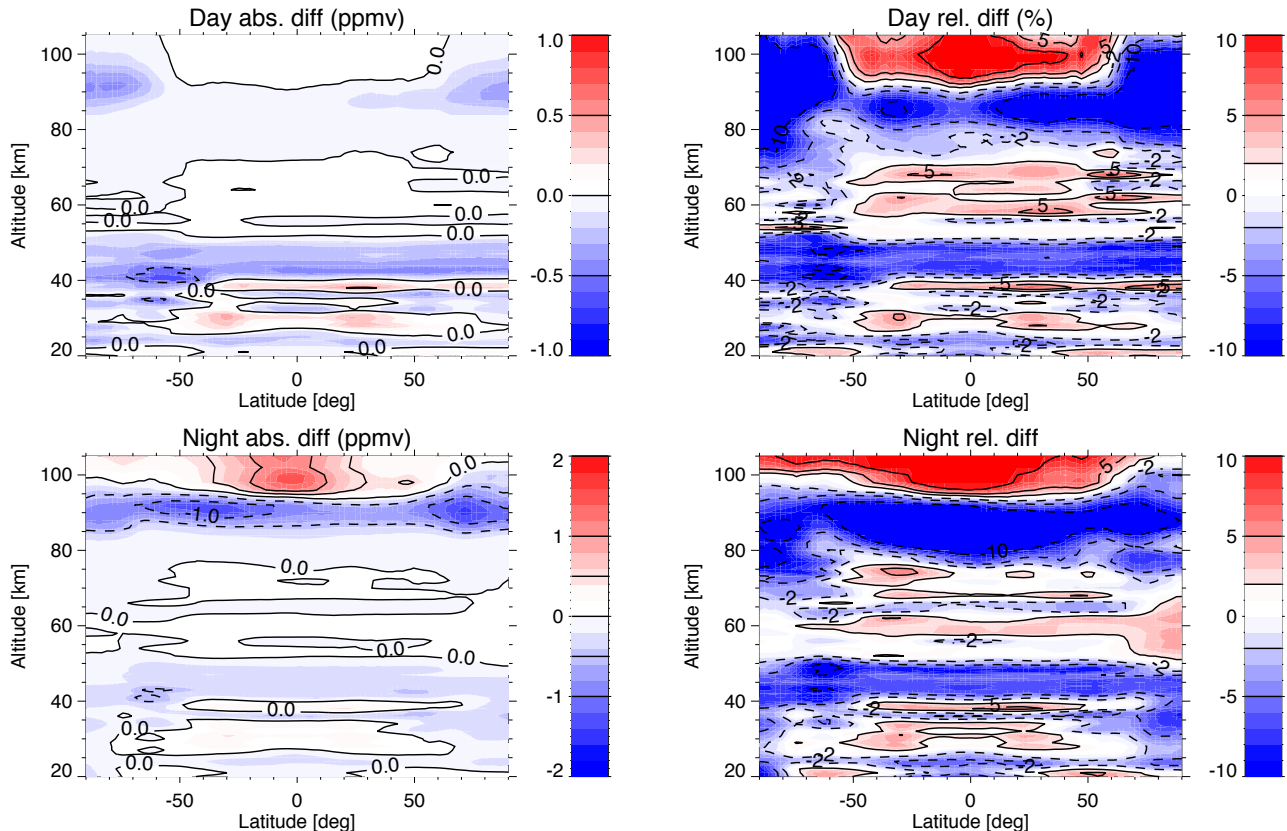
Figure 6. Comparison of O$_3$ abundance retrieved in the current V5r_O3_m22 with the previous V4O_O3_m02 version for daytime conditions (10 am) (top) and nighttime (bottom). The plots show the mean of the differences, in % of the older version, (V5r_O3_m22-V4O_O3_m02)/V4O_O3_m02, for all data taken in 2009.

5   Differences between current V5r_O3_m22 and previous V4O_O3_m02 versions

Since the previous V4O_O3_m02 version of MIPAS O$_3$ has been used in some previous studies, (e.g., Smith et al., 2013, 2014) it is interesting to compare those results with the vmrs of this new V5r_O3_m22 version. The V5r_O3_m22 ozone retrieval setup has been improved with respect to the earlier in the following aspects.

First, the MIPAS L1b spectra have been updated from version 4.61/62 to version V5 (5.02/5.06). The spectroscopic data were upgraded from the HITRAN database version of 2004 to that of 2008. The retrieved kinetic temperature from MIPAS has also been changed to the temperature version of v5r_TLOS_m21 (see major differences discussed above). We have also improved

the width of the integration window of the apodized instrument line shape function. The uppermost altitude of the continuum retrieval has been expanded from 30 to 50 km. The regularization scheme has been updated in order to make it compatible with that used in the nominal O_3 retrieval (von Clarmann et al., 2013) in the common altitude range (up to 70 km). The MWs have also been revised so below 50 km we only use MWs located in channel A (see Table 3), like in NOM retrievals. We use a

5 different distribution of the CO_2 abundance, now taken from WACCM (see above). The merging altitude of the daytime atomic oxygen derived from the ozone retrieval (assuming photochemical equilibrium) to the model (supplied for the region above) has been changed from 95 km to 97 km. At nighttime we need, additionally, the H concentration, which has been taken from the NRLMSIS-00 model (Picone et al., 2002). In the previous version we took the nighttime O from the NRLMSIS-00 model in the whole altitude range. Above 97 km we use now the atomic oxygen from WACCM instead of that of NRLMSIS-00.

10 An important update is the re-calculation of the O_3 vibrational temperatures during the iterations in the inversion process, following the update of the atomic oxygen. The O_3 non-LTE model has also been improved, as described above in Sec. 2.

The average impact on the ozone retrieval after those changes (see Fig.6) is an increase of 2-3% (0.2-0.5 ppmv) below around 40 km (except in the polar winter where there is a decrease). The clear increase around 40 km is due to the inclusion of the retrieval of the continuum for this altitude.

15 There is a clear decrease by $\sim$5-10% ($\sim$0.4-0.5 ppmv) between 40 and 50 km principally induced by the use of micro-windows in channel A only (MWs in channel AB for these altitudes were removed). In the lower and middle mesosphere, 50-80 km, there is an increase of about 2-5% (0.1-0.2 ppmv). In the upper mesosphere, there is a general decrease of $\sim$0.5-1 ppmv at nighttime conditions, principally caused by neglecting the removal of the excited $O_3(v_3)$ by chemical reaction with atomic oxygen. This produces a larger population of $O_3(v_3)$ and hence less O_3. At daytime the effect is much smaller and

20 has a smaller impact on the retrieved ozone (in absolute values). At altitudes above around 95 km, the O_3 in the new version is larger by about 5-10%. This is caused by the use of the atomic oxygen from the WACCM model, which is larger than in NRLMSIS-00 and even overcomes the smaller relaxation of $O_3(v_3)$ due to the chemical relaxation being ignored.

6   Validation

We have compared MIPAS V5r_O3_m22 ozone retrievals with co-located measurements from SABER, GOMOS, MLS,

25 SMILES and ACE-FTS. Comparisons for GOMOS are only for night conditions and in number density. For ACE-FTS, because it is an occultation instrument and O_3 has very large diurnal variations around the terminator in the middle and upper mesosphere, we compare ACE sunset and sunrise with MIPAS observations with solar zenith angles (SZA) in the range of 88 to 92°. In order to select a pair of profiles to compare, we have selected measurements with Universal Time differences smaller than 2 h and distances smaller than 1000 km. Considering an additional criterion of 1 h local time difference did not change the

30 results significantly.

6.1 Instruments

6.1.1 SABER

The Sounding of the Atmosphere using Broadband Emission Radiometry (SABER) is a broadband radiometer flying onboard the NASA's Thermosphere-Ionosphere-Mesosphere Energetics and Dynamics (TIMED) satellite, launched on December 2001 and starting operations in January 2002 (Russell III et al., 1999). SABER measurements cover 83°S to 52°N and from 52°S to 83°N, alternatively every two months. A 24-h local time coverage is completed approximately in 60 days. SABER observes the daytime and nighttime ozone limb emission at 9.6 μm, from which the ozone concentration is retrieved under non-LTE conditions from 10 to 100 km. We use here version 2.0 ozone, publicly available at http://saber.gats-inc.com. The non-LTE model used in SABER ozone retrievals is described in Mlynczak et al. (2013) and references therein. Similar to MIPAS, the retrieval of O_3 from SABER requires knowledge of pressure, temperature and atomic oxygen. The first two are taken from SABER retrievals of simultaneous measurements at 15 μm (Remsberg, 2008; García-Comas et al., 2008). The atomic oxygen for SABER ozone retrievals is taken from the US Naval Research Laboratory- Mass Spectrometer and Incoherent Scatter Radar model (Picone et al., 2002). SABER ozone retrieval additionally needs to include the contribution of one CO_2 laser band emission in the ozone channel. For that it uses the CO_2 vibrational temperatures computed during the SABER temperature retrieval. The vertical resolution of SABER ozone is approximately 2 km. Given MIPAS O_3 coarser vertical resolution, particularly in the mesosphere, we used the MIPAS averaging kernels and a priori O_3 to smooth SABER O_3 profiles. Rong et al. (2009) reports SABER ozone precision of $\approx 1 - 2\%$ in the stratosphere and $\approx 3 - 5\%$ in the lower mesosphere. The systematic errors range from 22% in the lower stratosphere to $\approx 10\%$ in the lower mesosphere.

Previous comparisons between SABER v1.07 and MIPAS V4O_O3_m02 ozone vmrs in the mesosphere were performed by Smith et al. (2013). These showed the largest differences at the secondary maximum, which were attributed to the coarser MIPAS vertical resolution. They also mentioned that differences arose from the different SABER and MIPAS pressure/temperature profiles which affected conversion from density to vmr. The differences between SABER version 1.07 used in Smith et al. (2013) and version 2.0 (used here) are small (Smith et al., 2014).

6.1.2 GOMOS

The Global Ozone Monitoring by Occultation of Stars (GOMOS) was a stellar occultation spectrometer onboard the ESA's Envisat space platform (Bertaux et al., 2010). It operated from August 2002 to April 2012. Ozone density profiles are derived from GOMOS UV-visible measurements at $250-692$ nm from 10 to 110 km. GOMOS provides nighttime observations that are performed at around $22-23$h LST at low latitudes. The latitudinal coverage eventually reaches the poles and slightly varies throughout the year due to varying distribution of stars used in the observations. The dataset used here was retrieved using ESA Instrument Processor Facility (IPF) version 6.01, described in Kyrölä et al. (2010) and Sofieva et al. (2010), and is available under registration at the ESA Earth online portal (https://earth.esa.int). Unreliable profiles in the dataset have been screened out following recommendations of the GOMOS/6.01 Level 2 Product Quality Readme file. The user-friendly version of the GOMOS dataset (HARMOZ, Sofieva et al., 2013), which is screened for invalid data, is in an open access at the

Ozone_cci web-page, http://www.esa-ozone-cci.org/?q=node/161. The vertical resolution of GOMOS ozone varies from 2 km in the lower stratosphere to 3 km in the upper stratosphere and above. Being better than the MIPAS vertical resolution, we have used MIPAS averaging kernels to smooth GOMOS profiles. Since GOMOS provides O_3 number density but not O_3 vmr we compare GOMOS and MIPAS O_3 number densities. Random errors due to measurement noise and scintillations are $0.5-4\%$ in the stratosphere and $2-10\%$ in the mesosphere. Systematic errors are smaller than 2% and they are mainly due to O_3 cross sections (Tamminen et al., 2010).

6.1.3 MLS

The Microwave Limb Sounder (MLS) was launched on July 2004 on the NASA's Earth Observing System Aura satellite (Waters et al., 2006). The equatorial crossings occur at 1:43/13:43 LT and the latitudinal coverage is between 82°S and 82°N. Daytime and nighttime ozone profiles are derived from measurements of its thermal limb emission at 235.71 GHz from the troposphere to ≈90 km. However, its usable range is up to 0.02 hPa or ∼72 km (see https://mls.jpl.nasa.gov/products/o3_product.php). The ozone dataset used here is version 4.2, downloaded from GES DISC (Schwartz et al., 2015) and described in Livesey et al. (2017) and references therein. The vertical resolution is 3 km in the stratosphere, 6 km in the middle mesosphere and 9 km in the upper mesosphere. MLS ozone has generally indicated 5-10% agreement with other datasets in the stratosphere. The estimated systematic uncertainty is 5-10% in the stratosphere, 10-20% in the lower mesosphere and 20-50% in the middle mesosphere Livesey et al. (2017). Due to the larger MLS O_3 vertical resolution in the mesosphere, we have applied MLS averaging kernels and a priori information to the MIPAS ozone.

6.1.4 SMILES

The Superconducting Submillimeter-Wave Limb-Emission Sounder (SMILES) was attached to the Exposed Facility of the JAXA's Japanese Experiment Module (JEM) of the International Space Station (ISS) and operated between October 2009 and April 2010 (Kikuchi et al., 2010). It measured ozone profiles from 16 to 85 km during daytime and to 96 km during nighttime, derived from measurements between 625 and 651 GHz using the technique described in Mitsuda et al. (2011), Takahashi et al. (2010), and Takahashi et al. (2011). The latitudinal coverage is 38°S and 65°N. We use here data version 3.2, available at the Data Archives and Transmission System (DARTS) site (http://darts.isas.jaxa.jp/stp/smiles/). The vertical resolution is 3 km in the stratosphere, 4 km in the lower and mid-mesosphere and 6 km at 95 km. MIPAS and SMILES O_3 vertical resolutions are similar and hence we did not apply averaging kernels to any of them. Previous versions of SMILES O_3 (v2.2) agree with other measurements within 10% in the stratosphere and 30% in the mesosphere (Imai et al., 2013a, b).

6.1.5 ACE-FTS

The Fourier Transform Spectrometer (ACE-FTS) is an infrared solar occultation Michelson interferometer flying on the CSA's Atmospheric Chemistry Experiment (ACE), also called Science Satellite (SciSat), launched in August 2003 (Bernath, 2017). It measures atmospheric absorption from the cloud top to 150 km during sunrise and sunset. The ACE orbit's high inclination results in coverage of the tropical, mid-latitude and high-latitude regions over approximately three months. Ozone profiles are

derived from measurements at several microwindows between 829 and 2673 cm^{-1} using the methodology described in Boone et al. (2013). We use here data version 3.5. The retrievals are limited to the altitude range of 5 to 95 km. The vertical resolution is 3−4 km. The ACE-FTS version 3.5 O$_3$ product agrees with MLS measurements to within +4% from 20-45 km. Compared to MLS, it exhibits a positive bias of up to 18% between 45 and 60 km and an increasing negative bias at higher altitudes (Sheese et al., 2017).
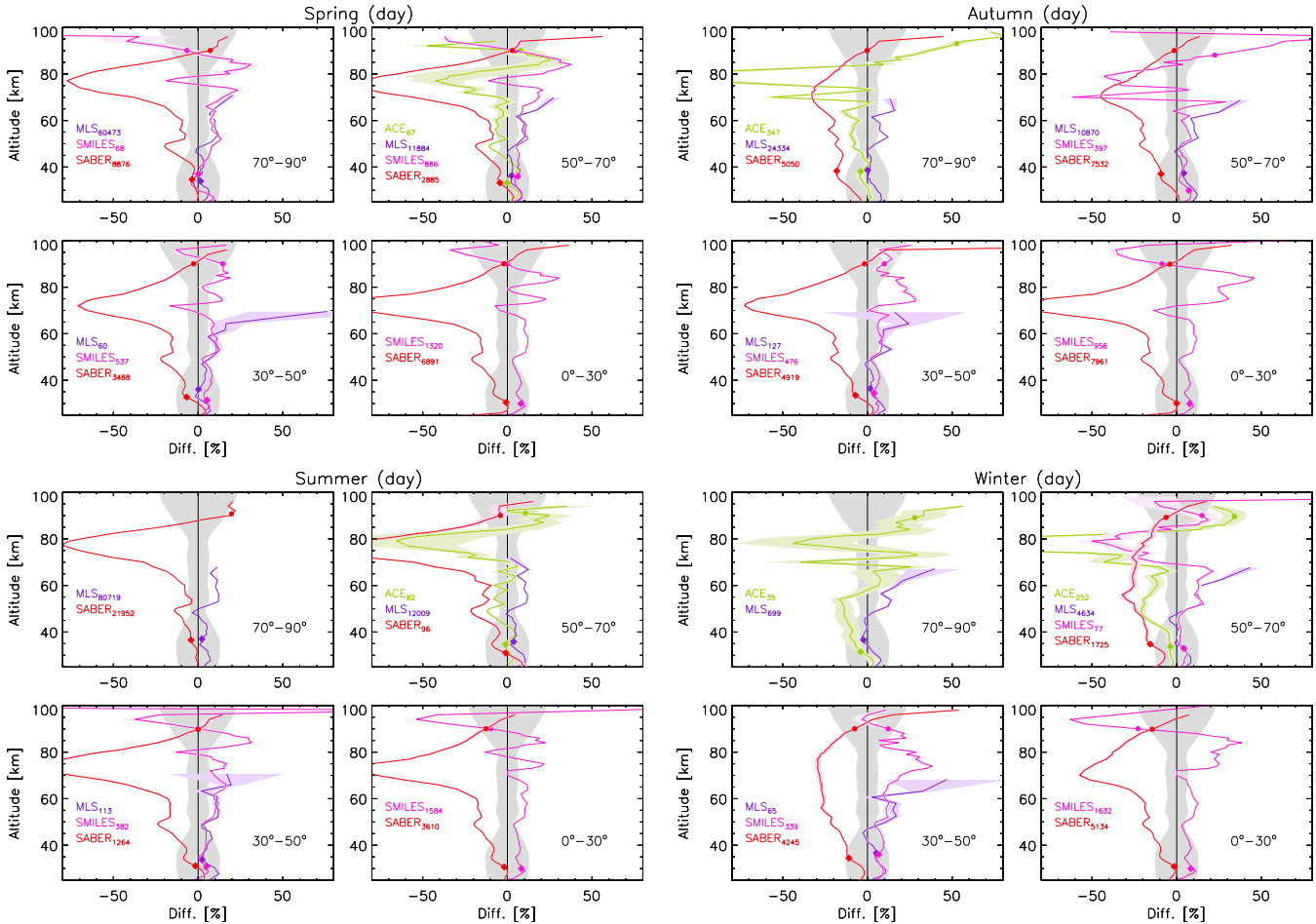
Figure 7. Mean of the daytime O$_3$ vmr differences (MIPAS–instrument) in % of MIPAS between co-located pairs of measurements of MIPAS (MA mode) with ACE-FTS (green), SABER (red), MLS (purple), and SMILES (magenta) for spring (MAM for NH and SON for SH) (upper/left quadrant), autumn (SON for NH and MAM for SH) (upper/right quadrant), summer (JJA for NH and DJF for SH) (bottom/left quadrant), and winter (DJF for NH and JJA for SH) (bottom/right quadrant). The symbols indicate the mean altitude of the MIPAS O$_3$ vmr primary (diamonds) and secondary (circles) maxima coincident with the respective instrument. The numbers of coincidences are indicated in the subscripts. The grey shaded area shows the MIPAS systematic errors. The color-shaded areas (hardly noticeable in many cases) are the standard errors of the mean of the differences.
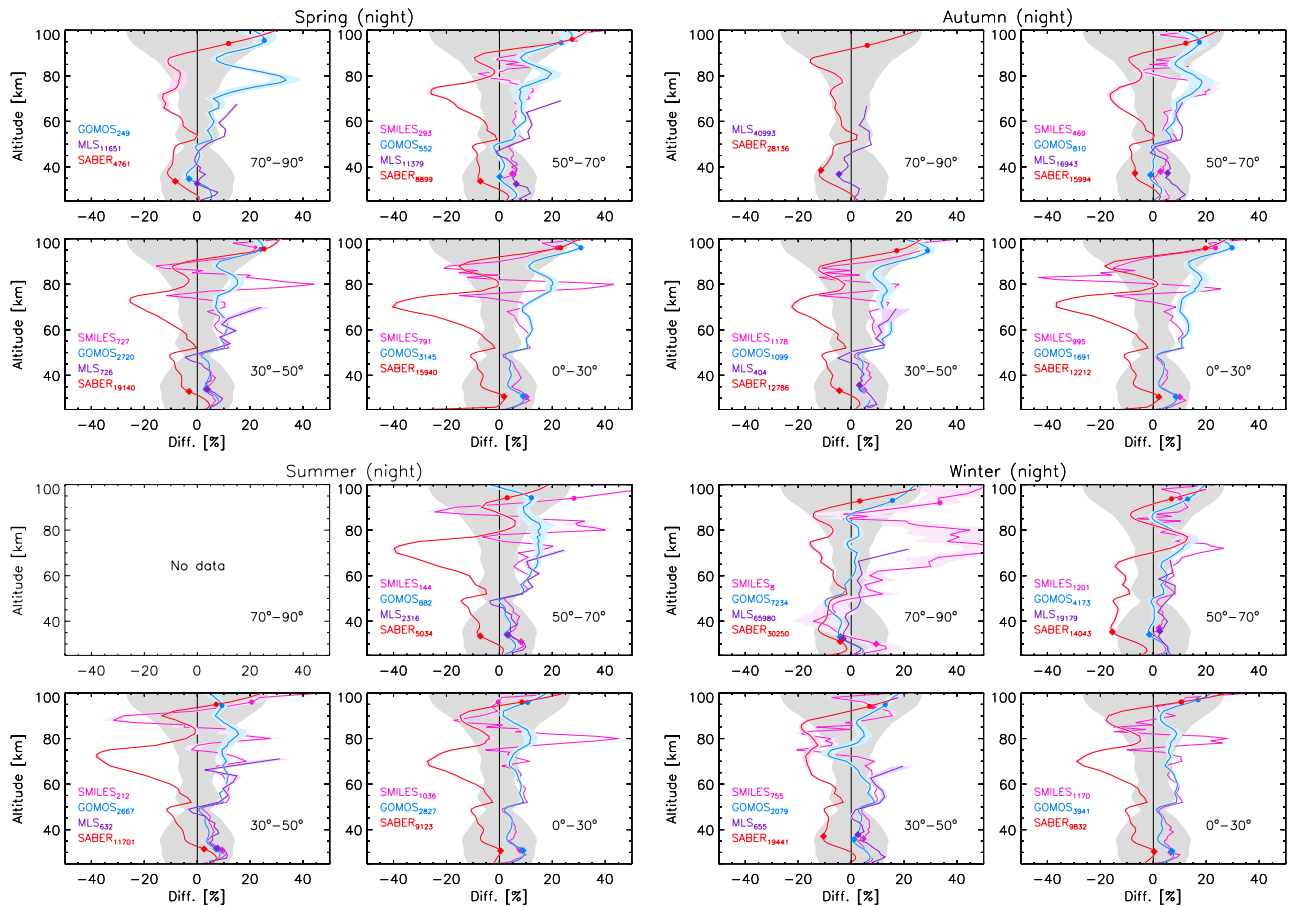
Figure 8. As Fig. 7 but for nighttime O_3. Instruments colors are the same except that ACE-FTS is replaced by GOMOS (light blue).

6.2 Results of comparisons

Figures 7 and 8 show the mean daytime and nighttime differences, respectively, between MIPAS and the different instruments (MIPAS−instrument) for the four seasons, grouped in four latitude bins. In addition, Figs. 9 and 10 show the global means, for all latitudes and seasons, for daytime and nighttime, respectively. The number of co-located pairs included in each mean

5   difference profile is indicated as a subindex in the instrument's label. The mean altitude of the MIPAS O_3 vmr primary and secondary maxima, coincident with the respective instrument, are also plotted as additional information.

In general, the agreement with all instruments, except SABER, is better than 5% below 50 km in all seasons for both daytime and nighttime; MIPAS O_3 being larger (see Figs. 9 and 10). The differences around the ozone primary maximum (diamonds in the figures) are smaller than 5%. These differences are well within MIPAS systematic errors (see Table 4). However, MIPAS

10   (as the other instruments) measures less ozone than SABER below 50 km, with values of 10-20% from 30 to 50 km and 5-15% at the stratospheric O_3 maximum.
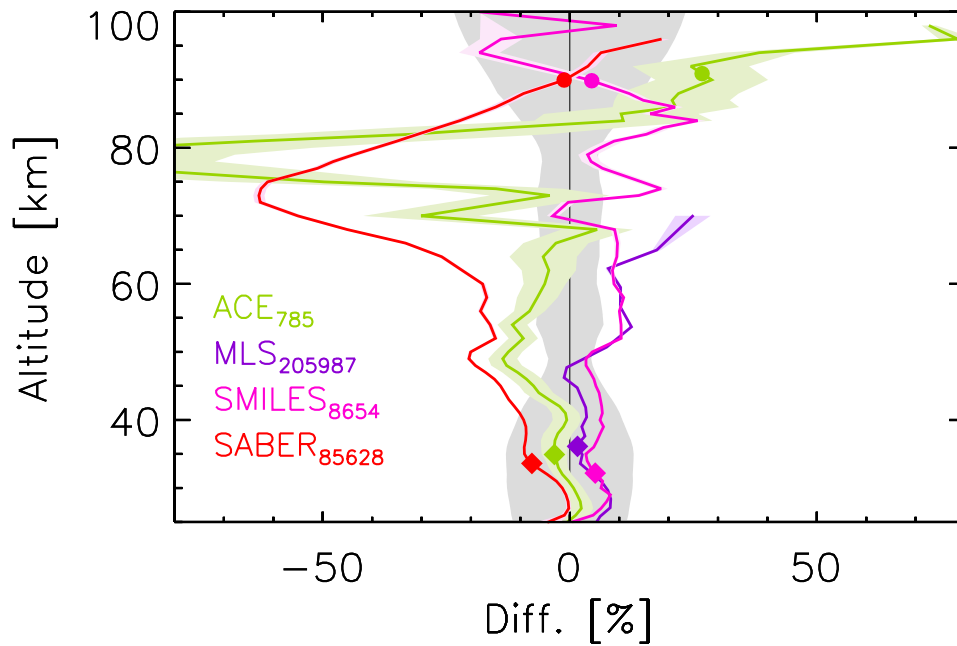
Figure 9. Global mean (for all latitudes and seasons) of the daytime O_3 vmr differences (MIPAS–instrument) in % of MIPAS between co-located pairs of measurements of MIPAS (MA mode) with ACE-FTS (green), SABER (red), MLS (purple), and SMILES (magenta). For more details see caption of Fig. 7.
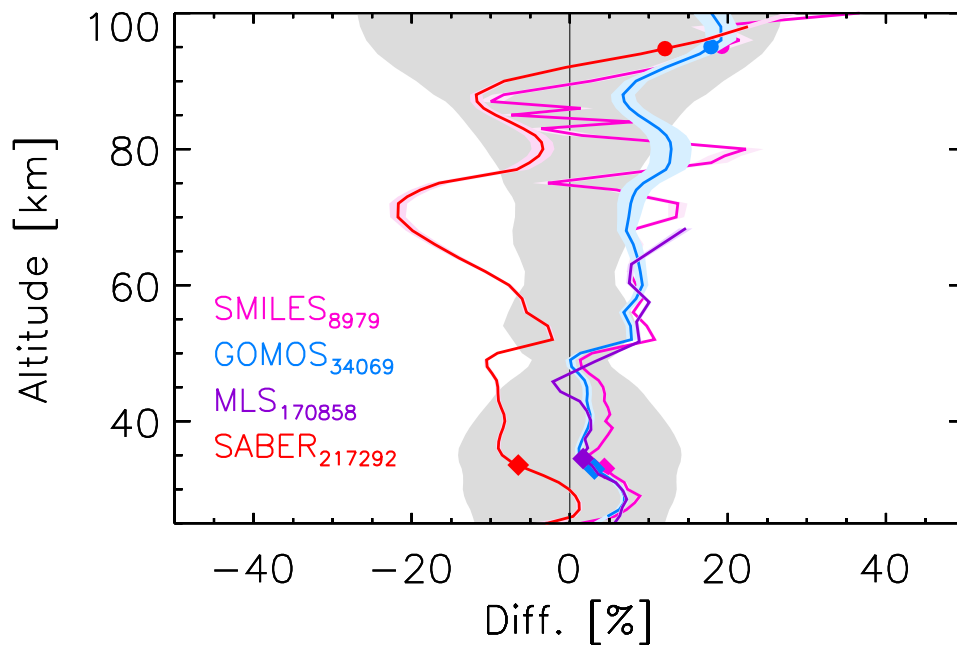
Figure 10. As Fig. 9 but for nighttime O_3. Instruments colors are the same except that ACE-FTS is replaced by GOMOS (light blue).

At altitudes from 50 to 65-70 km, we also find a good general agreement with all instruments, except SABER at 60–70 km, and MLS at 65–70 km in some latitudes/seasons. The differences are smaller than 5-10% in all seasons both during daytime and nighttime, with MIPAS O_3 generally being larger (see Figs. 9 and 10). These differences are within or just at the edges of the MIPAS systematic errors (grey shading in the figures). Opposite to that behaviour, MIPAS is smaller (5–10%) than ACE-FTS in the altitude range of 45–55 km (see Fig. 9). This is likely the effect of the known positive bias of ACE-FTS O_3 in this region (Sheese et al., 2017). MIPAS measures up to 10% (nighttime) and up to 20% (daytime) less ozone than SABER from 50 to 60 km. These differences increase above 60 km and are discussed below.

Exceptions to that general behavior are the larger differences found with MLS at 65-70 km at daytime in spring (at 30°-50°) and autumn and winter for most latitudes. Differences with SMILES are also exceptionally larger at 60–80 km during nighttime in winter at 70°-90° but, with only 8 coincidences, they are not statistically significant.

A positive bias in SABER stratospheric O_3, version 1.07, was previously reported by Rong et al. (2009). Differences in temperature cannot explain this bias because they are 1–2 K larger than MIPAS below 30 km (which would result in less O_3) and are in excellent agreement (within 1 K) from 30 to 85 km (García-Comas et al., 2014). Some tests have shown the retrieval of MIPAS O_3 at these altitudes using MWs in the AB channel, e.g. the 10 μm spectral region where SABER measures, results in an 10% ozone increase (see Sec. 5 and Fig. 6). Thus, O_3 spectroscopic errors in the 10 μm region could be the reason for the larger SABER stratospheric ozone. Indeed, MIPAS and SABER measurements have a better agreement at 50 km (altitude above which MIPAS uses AB channel MWs) than at lower altitudes, whereas MIPAS differences with instruments other than SABER increase to 10% above that altitude.

Between 50 and 85 km MIPAS and SABER ozone profiles show similar vertical gradients but shifted (not shown). In this region ozone decreases with altitude to very small values and hence the relative differences are rather large. At 60–85 km they are within 20–80% at daytime, and 10–40% at nighttime, MIPAS ozone being smaller. A daytime SABER ozone overestimation at these altitudes was already reported by Smith et al. (2013). A likely explanation for the larger SABER O_3 values could be the faster de-activation of the O_3 v_1 and v_3 manifold by N_2 and O_2, $k_{vt,M}$ in Table 1. According to Mlynczak et al. (2013), the SABER retrieval uses the values reported by Martin-Torres (1999) which are about a factor of 2 faster than those measured by Menard et al. (1992) which are used here. A faster collisional rate gives rise to smaller $O_3(v_3)$ vibrational temperatures and hence to larger retrieved O_3 vmr. The fact that the non-LTE deviation of $O_3(v_3)$ vibrational temperatures from the kinetic temperature is larger at daytime than at nighttime could explain the larger daytime bias.

MIPAS differences with other instruments are larger above 70 km than below. These differences are of 10–20% with SMILES and GOMOS (nighttime). When compared with ACE-FTS, MIPAS O_3 is significantly smaller ($<-50\%$) near 80 km (see Fig. 9). This large relative difference is in part caused by the very small values of O_3. The difference in absolute values is smaller than 0.1 ppmv. Also, the difference could be due to different solar illuminations along the LOS of both instruments.

In the polar winter around 70 km, where the tertiary maximum develops (see Sec. 7), MIPAS agreement with GOMOS is excellent (3%) (see Fig. 12, winter at 70-90°). MIPAS and GOMOS lie between the rest of the other instruments, being on average 10% smaller than SABER (night), 20% larger than MLS (during night), within $\sim$30% of ACE-FTS (terminator) and 50% larger (although with a very few coincidences) than SMILES (night). Smith et al. (2013) reported that SABER version

1.07 O_3 did not exhibit a tertiary maximum, which contrasts with version 2.0 where SABER shows the largest ozone tertiary maximum of all the instruments considered.

At altitudes above 85–90 km during nighttime the differences increase with altitude and are generally larger. In the case of MIPAS and SABER the differences are partially due to a vertical shift of 1–2 km (not shown).

At the altitude of the secondary maximum, the agreement between all instruments for daytime conditions, is very good, except ACE-FTS in autumn and winter. MIPAS daytime ozone differences with SABER and SMILES are within 5 and 10%, respectively, except for low latitudes in the solstices (10%) and summer high latitudes (20%) for SABER, and autumn high latitudes and winter low latitudes (20%) for SMILES. MIPAS ozone is generally larger than that of ACE (by a mean of $\sim$20–30%) at this altitude. This difference can be partially due to the different illumination conditions along the LOS of both instruments. Actually we performed a test, restringing MIPAS data to SZA$<$85°, and the difference was reduced to just 10% (0.2-0.3 ppmv).

During nighttime, however, MIPAS ozone is between 5% and 25% larger than the other instruments around the secondary maximum. The differences somehow vary with season, being largest in spring and autumn. MIPAS ozone is 10–20% larger than SABER and SMILES, and 10-25% larger than GOMOS.

At altitudes above around 93 km, this larger MIPAS nighttime ozone is most likely caused by the large atomic oxygen in WACCM. If using the MSIS atomic oxygen in this region those differences would be reduced by 10–15% (see Figs. 7 and 8).

Overall, focusing on Figs. 9 and 10, MIPAS O_3 has an accuracy better than 5% at and below 50 km, with a positive bias of only a few percent. In the 50-75 km region, MIPAS O_3 has a positive bias of approximately 10%, possibly caused by spectroscopic errors. Between 75 and 90 km, nighttime MIPAS O_3 is within 10% of SABER and SMILES O_3 but has a positive bias of about 10% with respect to GOMOS. In this region, during daytime, the relative differences are larger, with a positive difference of 10–20% with SMILES, and negative difference of 10–50% with ACE and SABER. Given that ACE measures at the terminator and SABER daytime O_3 has a known positive bias, we think that MIPAS O_3 in this region is accurate to within 10-20%. Above 90 km, MIPAS O_3 at daytime is in agreement with other instruments by 10%. At nighttime, however, it shows a positive bias increasing from 10% at 90 km to 20% at 95-100 km, which is attributed to the large atomic oxygen of WACCM.

7 Climatology

The MIPAS middle atmosphere O_3, with a global (pole-to-pole) latitude coverage, day and nighttime measurements taken at two fixed local times, and spanning the altitude range from 20 to 100 km, represents a very important dataset for studying the middle atmosphere. In this section we present some ozone distributions, represented versus altitude, latitude and time, showing the major O_3 features in the middle and upper mesosphere.

Figures 11 and 12 show composite monthly zonal means of MIPAS O_3 data for the 2007-2012 period for day- and night-time, respectively. Here we consider "daytime" the measurements with a solar zenith angle (SZA) smaller than the SZA of the terminator, $SZA_{ter}(z) = 180 - \arcsin(R_\oplus/(R_\oplus + z))\,180/\pi$ ($R_\oplus$ is the Earth's radius and z is altitude) decreased in 3°, and taken at 10 am local time. The decrease in 3° was done to avoid scans partially in dark conditions. "Nighttime" is taken when
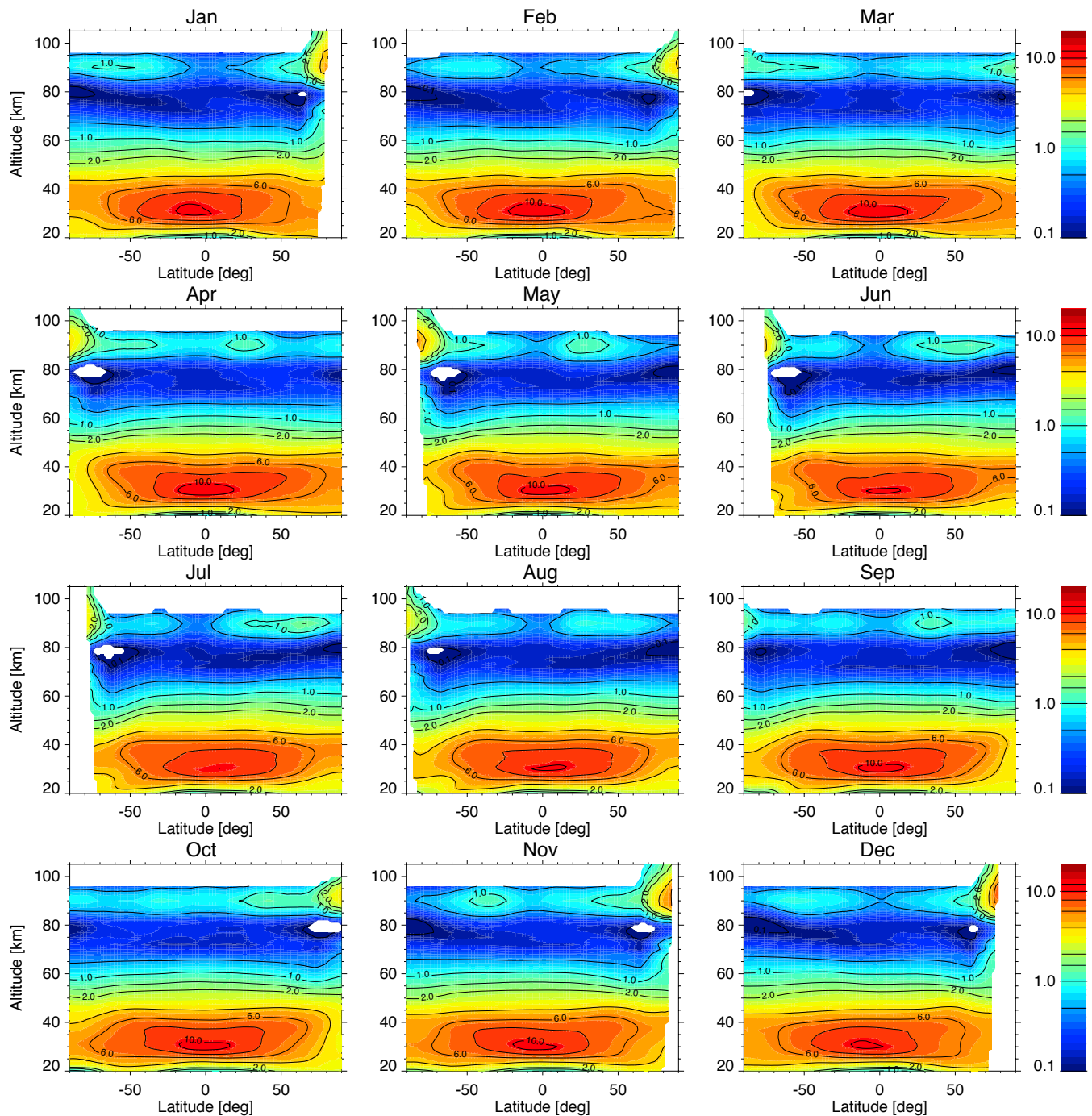
Figure 11. Composite monthly zonal mean of MIPAS data taken in the MA mode for the 2007-2012 period for daytime (local time of 10 am). White areas denote regions where MIPAS has no sensitivity to measure the very low ozone values. Contours are 0.1, 0.5, 1, 1.5, 2, 4, 6, 8, 10 and 12 ppmv.
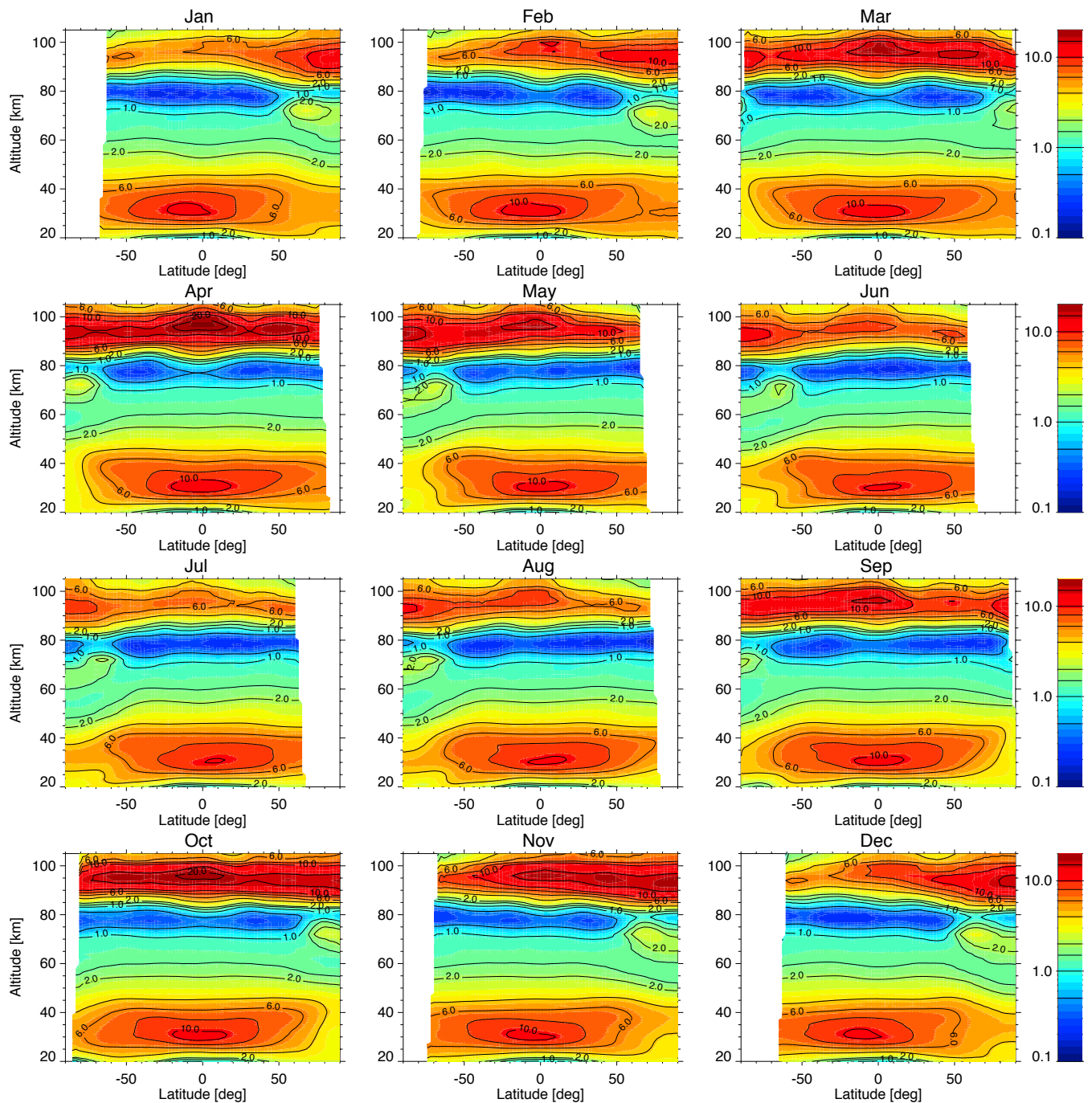
Figure 12. Composite monthly zonal mean of MIPAS data for the 2017-2012 period for nighttime. Contours are 0.5, 1, 1.5, 2, 4, 6, 8, 10, 15, and 20 ppmv.
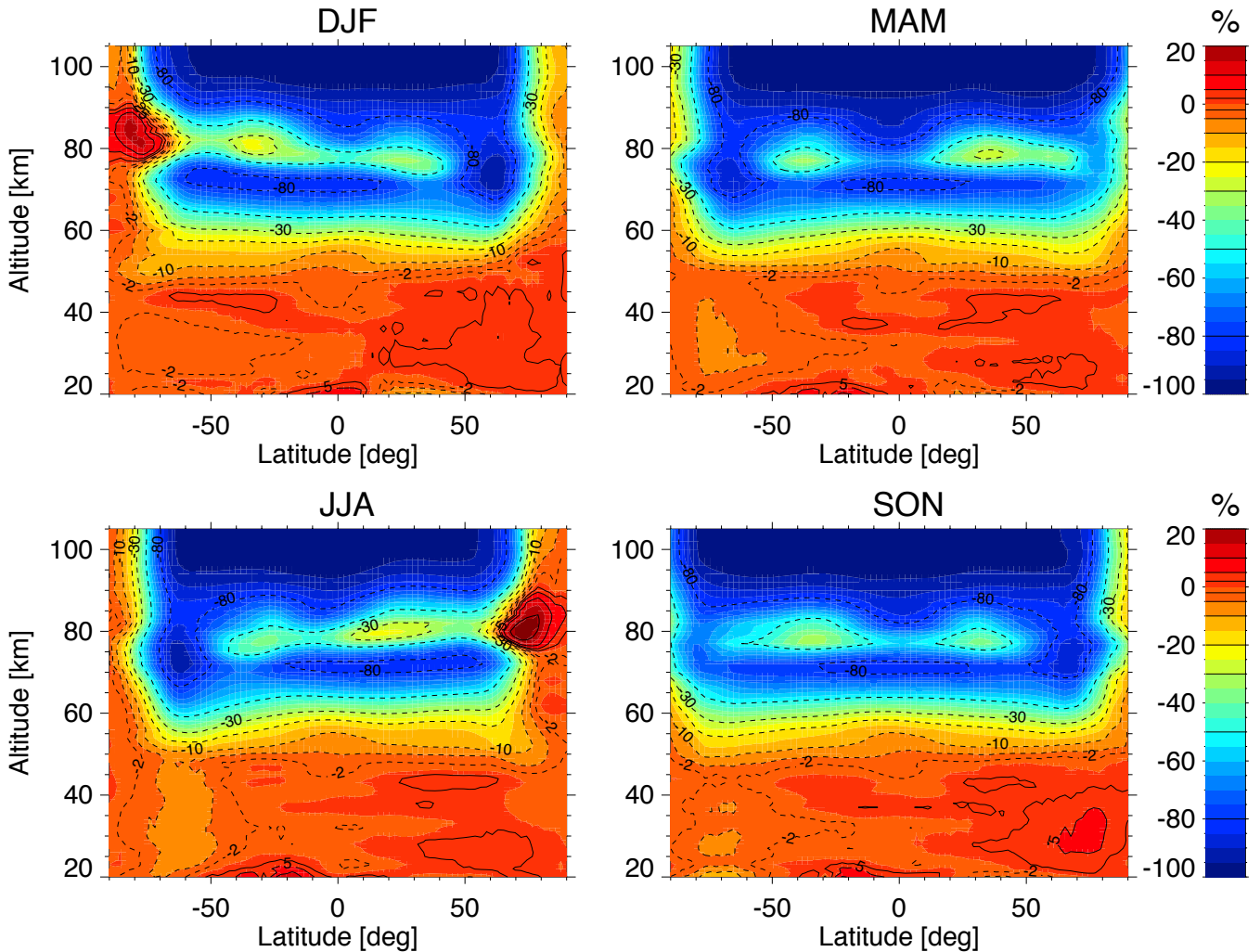
Figure 13. Composite seasonal zonal mean of O_3 diurnal differences (10 am–10 pm in percentage of 10 pm) of MIPAS data taken in the MA mode for the 2007-2012 period. DJF stands for December, January and February; MAM for March, April and May; JJA for June, July and August; and SON for September, October and November. Contours are -80, -50, -30, -20, -10, -5, -2, 2, 5, 10 and 20%.

the observed altitude is in dark conditions, $SZA(z) > SZA_{ter}(z)$, and the measurements are taken at a local time of 10 pm. Those figures show the typical primary, secondary and tertiary maxima and their seasonal evolution.

The latitudinal/seasonal distribution of daytime O_3 in the secondary maximum, near 90-95 km, shows maxima near the polar winters (November-February in the NH, and May-August in the SH) (Fig. 11).

5   In general we observe a minimum in the daytime O_3 secondary maximum near the tropics (except perhaps for October) which is attributed to tidal effects (see, e.g., Marsh et al., 2002; Dikty et al., 2010). The diurnal tertiary maximum, taking place usually around 60-75 km (Fig. 11), occurs during the winter seasons polewards of 60-70°.

The ozone secondary maximum at nighttime presents larger values near the polar winters, more precisely in the early polar winters (e.g. November in the NH and May in the SH). This polar winter maximum decreases as the season progresses in both hemispheres, and starts recovering near the end of the winter (February in the NH and August in the SH). This is in agreement with the results reported by Smith et al. (2014). These investigators have shown that this O_3 enhancement is caused by the relatively weak meridional circulation at those times/regions which leads to low temperatures and low H concentrations, both favouring the production of O_3.

Thus, during solstice, the O_3 secondary maximum shows a clear latitudinal gradient, growing from summer to winter. During the equinox months, the nighttime secondary maximum exhibits large O_3 values across all latitudes, reaching the highest values in April and October. In the equinox months of March, April, September and October, the signature of the diurnal migrating tide is apparent near the equator. Larger values are found near the equator than at adjacent latitudes near 75-80 km, then smaller around 85-87 km, and larger again near 95 km. The signature is more clearly seen in April and October when the largest values of the ozone secondary maximum are observed at the equator near 95 km, reaching up to about 20 ppmv. The nighttime tertiary maximum has larger values than during daytime (see Fig. 12) and it is usually shifted equatorwards. These values are in good agreement with the measurements of the nighttime tertiary maximum measured by GOMOS (Sofieva et al., 2009). At latitudes poleward of the terminator it is usually displaced to lower altitudes. Although not clearly noticeable (because of the scale) in Fig. 12, the nighttime tertiary maximum is slightly larger in the NH than in the SH, as reported by Smith et al. (2017).

For completeness we also show the composite seasonal zonal mean of the MIPAS O_3 diurnal differences (10 am–10 pm in percentage of 10 pm) in Fig. 13. The day-night differences below about 50 km are very small, generally comprised between $\pm 2\%$. These differences are within the range of other measurements and model predictions, (see, for example, Schanz et al., 2014; Studer et al., 2014; Sakazaki et al., 2013; Parrish et al., 2014; Moreira et al., 2017). This overall good agreement in the MIPAS O_3 diurnal variation with other measurements supports the good quality of MIPAS data in this LTE region. Above about 45-50 km the effects of photodissociation start becoming important showing a decline in the daytime O_3 with respect to the nighttime at most latitudes (more pronounced near the tropics) and seasons except near the polar regions. The diurnal differences increase with altitude. At $\sim$80 km the day/night differences are mainly ruled by the nighttime O_3 variations, which are largely controlled by the semi-annual oscillation (SAO) (see below) and the tidal motions changing the atomic oxygen and hence O_3. In the polar summer terminator near 80 km, daytime O_3 at 10 am exceeds O_3 at 10 pm. Above 90 km, nighttime O_3 is significantly larger.

7.1 Annual variability

Figure 14 shows the annual variability as latitude$\times$ months cross sections of O_3 at different altitudes for daytime (left column) and nighttime (right column).

At 40 km MIPAS observes larger O_3 values in the tropics and mid-latitudes compared to the polar regions, and also lower values in the SH polar winter compared to the NH winter. Around the equator we observe slightly larger values during solstice conditions (January and July) than at equinox (April and October). Maximum values also occur at mid-latitudes (30–40°)
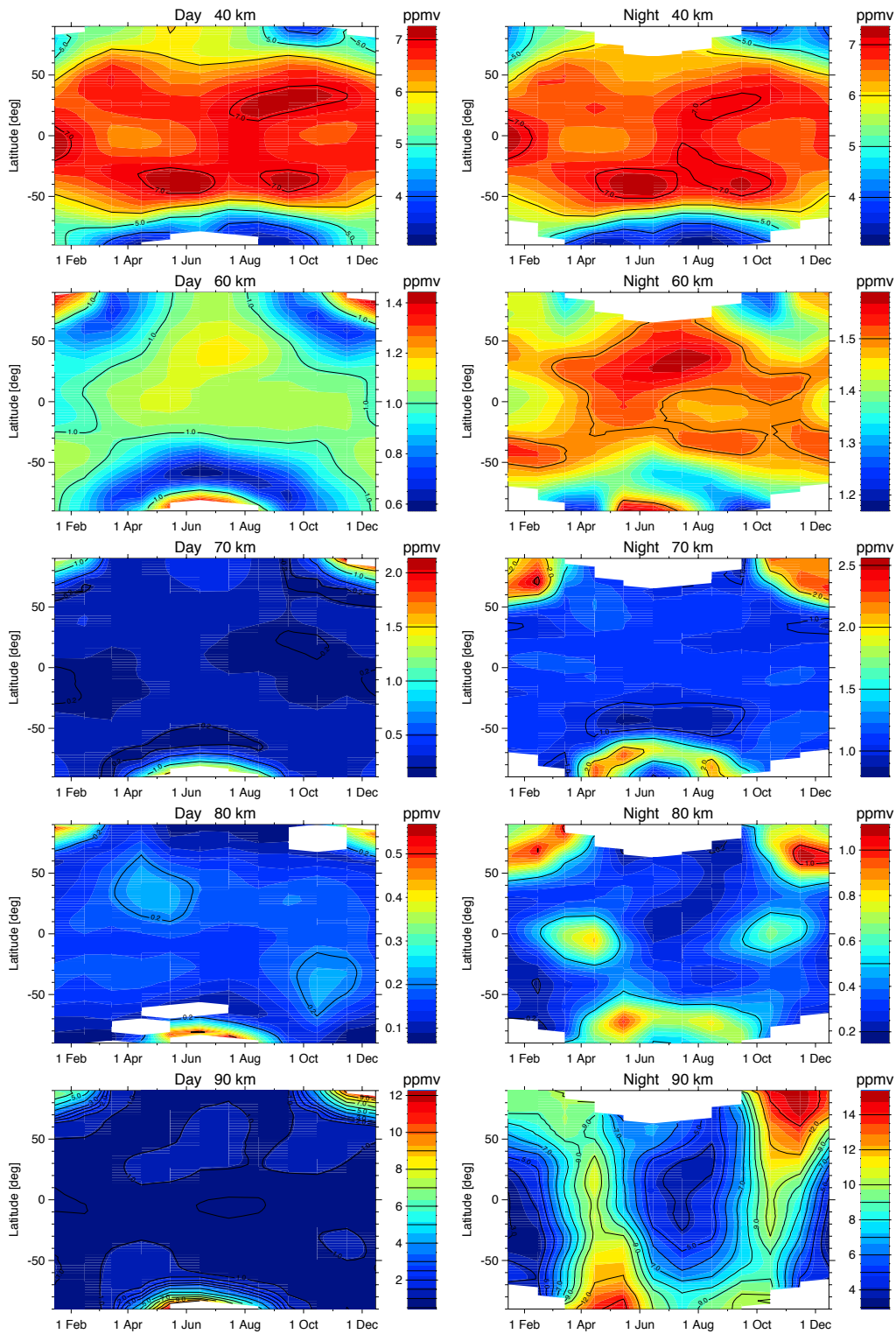
Figure 14. Seasonal evolution versus latitude of O_3 vmr at different altitudes for daytime (left row) and nighttime (right row). Note the different scales used in the different panels.

during May-June and September in the SH and during August and September in the NH. The day-night differences are small, with ozone slightly larger during daytime, more noticeable in the NH.

At 60 km the day-night differences are very marked, with smaller daytime ozone values due to losses by photo-dissociation. This pattern, due to illumination conditions, is very clear in the second panel of the first column.

At 70 km, the structure of the O_3 tertiary maximum (second column, third panel) in the SH polar winter is very obvious, exhibiting a "ring" shape following the terminator. The tertiary maximum has larger values in the early winter, then decreases and increases again at the end of the winter. Note also the higher values of the tertiary maximum in the NH polar winter (as discussed above). These results are consistent with the recent analysis of the tertiary maximum carried out by Smith et al. (2017).

The O_3 latitude × month distribution near 80 km shows during equinox conditions significant increases at mid-latitudes during daytime and in the tropics at nighttime, which seem to be caused by tides. Near the polar regions the nighttime O_3 at 80 km shows similar features to the tertiary maximum described above with larger values early in the winter in both hemispheres, and being larger in the NH.

At 90 km, the nighttime O_3 in the polar winter shows a more marked seasonal evolution than at lower altitudes, with much larger values in the early winter as has been shown by Smith et al. (2014). The semi-annual oscillation (SAO) is also evident in the tropics and at mid-latitudes (see, e.g., Garcia et al., 1997). Similar features have also been observed by GOMOS (Kyrölä et al., 2010). Even though O_3 has a short lifetime, and hence it is not significantly advected, its distribution responds to changes in temperature, atomic oxygen, and other species associated with the SAO. As a result of both effects ozone shows a kind of "U-shape" distribution at this altitude.

7.2 Altitude-resolved time series

In order to study the inter-annual variability We show in this section altitude-resolved time series of O_3 at the tropical and polar latitudes (Fig. 15); and as latitude×time cross sections at given altitudes (Fig. 16). We see clearly the semi-annual oscillation above around 75 km, both in day and nighttime in the upper panels of Fig. 15. We also observe in these panels that the O_3 secondary maximum is located at higher altitudes in nighttime than during daytime. In addition, there is a hint that the daytime O_3 secondary maximum shows the lowest concentrations close to the solar cycle minimum in 2009/2010, which is also visible in the bottom/left panel of Fig. 16.

Focusing on the polar regions (middle and bottom panels of Fig. 15), we observe that the stratospheric maximum (25-40 km) is slightly larger in the NH polar region than in the SH polar region. As discussed above, the nighttime tertiary maximum is slightly larger in the NH than in the SH polar region. In the SH it shows a double peak in each winter (early and late in the winter) while in the NH it is not so pronounced. Moving to higher altitudes, the nighttime O_3 secondary maximum shows a clear winter variability, with larger values early in the winter. The double peak structure appearing each winter is very evident in the SH hemisphere, as it is in the tertiary maximum, but not so clear in the NH hemisphere.
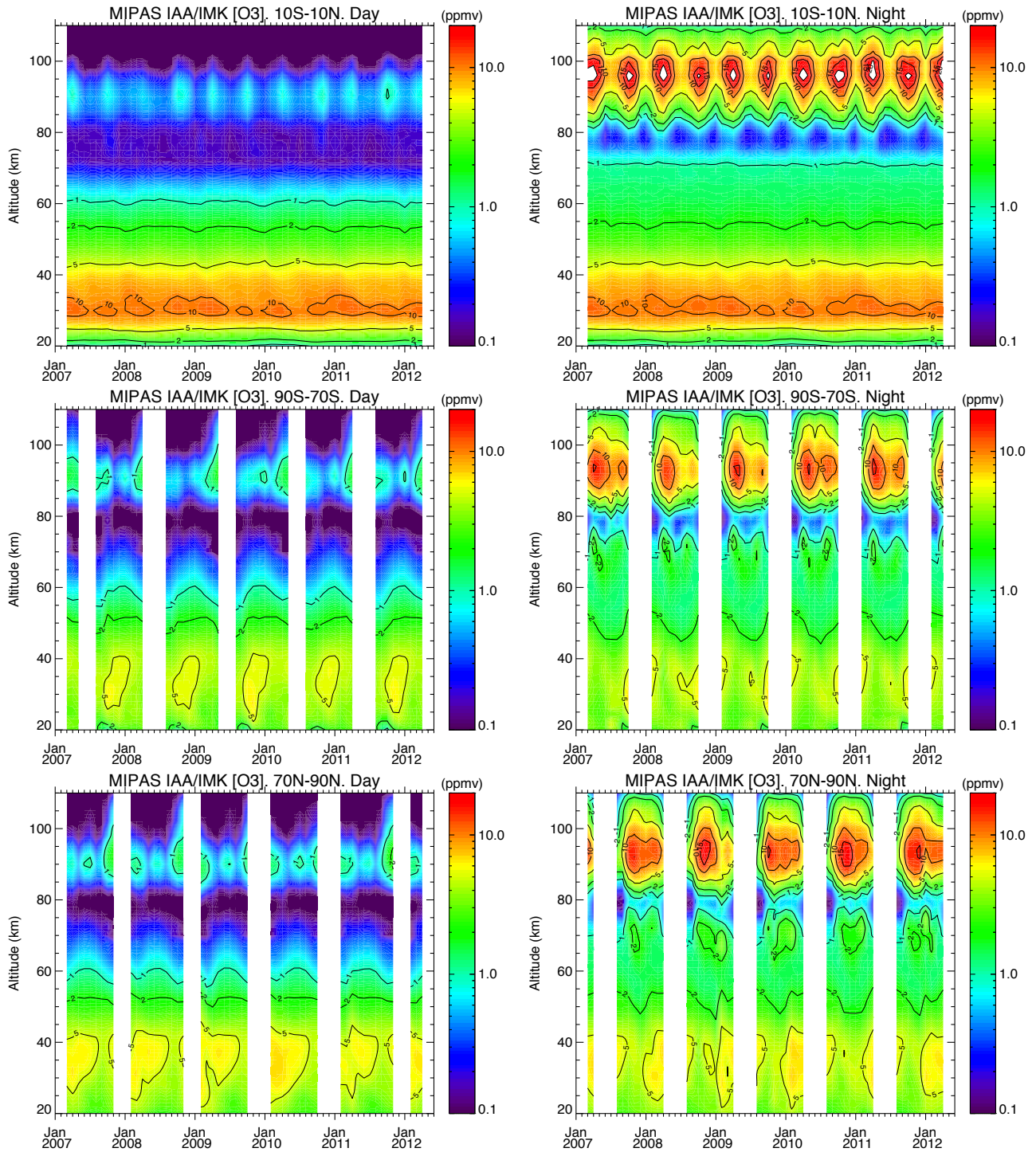
Figure 15. Altitude-resolved series, for latitudes near the equator (10°S-10°N) (top), the Southern polar region, 70°S-90°S, (middle) and the Northern polar region, 70°N-90°N (bottom), for daytime (left column) and nighttime (right column).
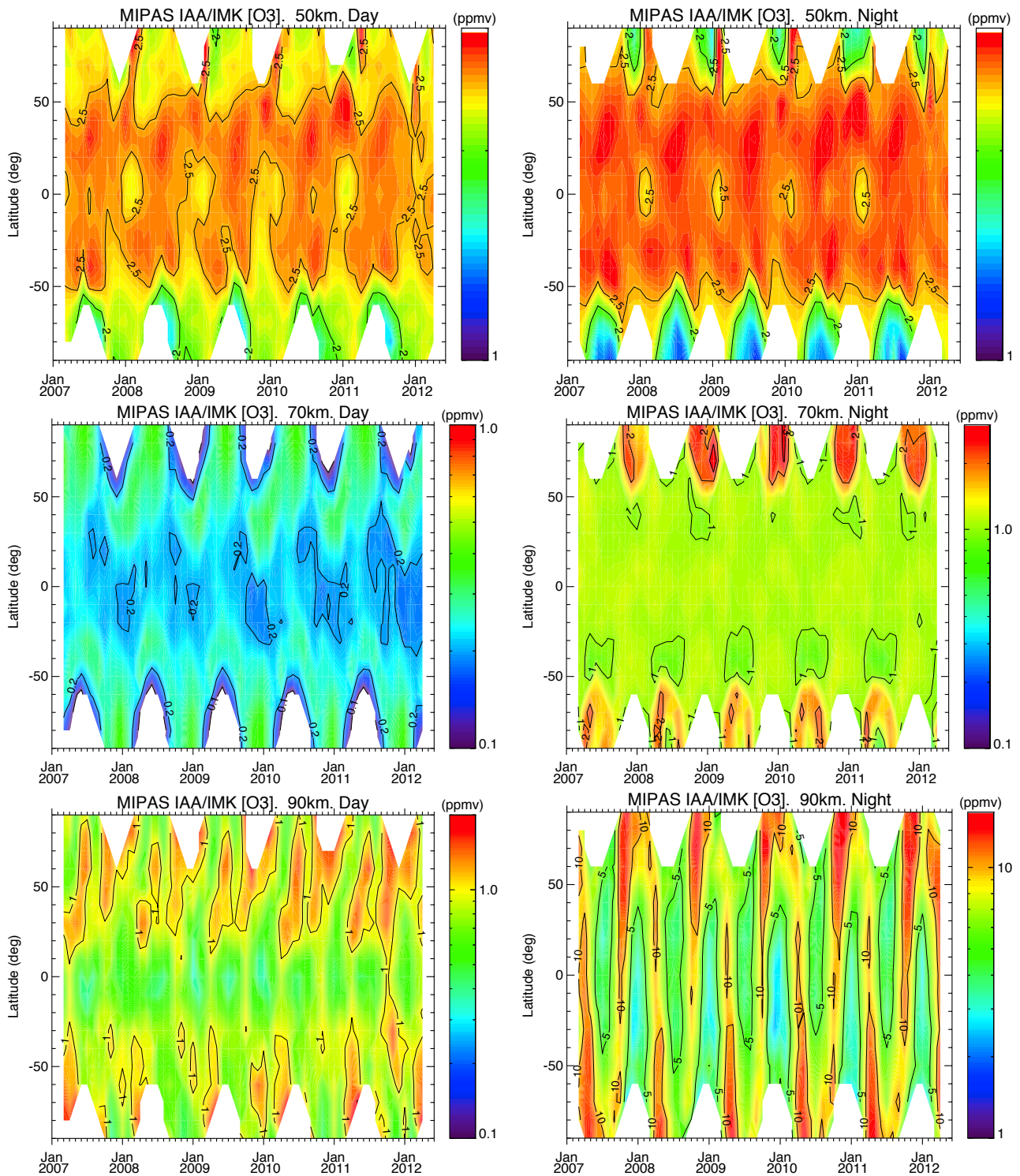
Figure 16. Cross section of latitude/time MIPAS O₃ at 50 km, 70 km and 90 km for daytime (left column) and nighttime (right column). Note the different color scales in some panels.

Figure 16 shows that the diurnal variation is clearly seen already at 50 km at the tropics and mid-latitudes, with slightly smaller values at daytime due to losses by photo-dissociation. This diurnal variation increases with altitude and at 70 km it is already quite large.

The presence of the tertiary maximum near 70 km at the polar regions leads to larger O_3 vmr values at these latitudes than at tropical and mid-latitudes, opposite to the latitudinal gradient shown at 50 km. In the middle/right panel of Fig. 16 we also observe that the nighttime tertiary maximum near 70 km is larger in the NH than in the SH hemisphere, as discussed above.

As described above, the bottom/left panel shows that the tropical daytime O_3 at 90 km shows lowest concentrations close to the solar cycle minimum in 2009/2010. This behavior is in concordance with model simulations (Marsh et al., 2007) and is explained by decreased odd oxygen production via O_2 photolysis at low solar activity conditions. The opposite occurs, however, at 70 km (middle/left panel), with a tendency to decrease towards 2012. Observational evidence for a negative solar ozone response at these altitudes has been provided by the analysis of Solar Mesosphere Explorer (SME) data on solar rotation time scales (Keating et al., 1987). Our observations suggest a long-term decline rather than a solar cycle variation since no O_3 increase before the solar minimum in 2009 can be identified. However, a clear attribution is not possible due to the relatively short observation period of MIPAS.

8 Summary and Conclusions

In this paper we describe the stratospheric and mesospheric ozone distributions (version V5r_O3_m22) retrieved from MIPAS observations in the three middle atmosphere modes (MA, NLC and UA) taken with an unapodized spectral resolution of $0.0625 \, cm^{-1}$ from 2005 until April 2012. The non-LTE modelling of O_3 is described in detail with emphasis on the unknown atmospheric and model parameters required to retrieve ozone from limb emission measurements near $10 \, \mu m$. In particular we discuss the role of atomic oxygen, which can be obtained during daytime by assuming it is in photochemical equilibrium with the retrieved O_3, but it is a source of uncertainty at nighttime.

We succinctly described the retrieval method and update the O_3 non-LTE model parameters and the new microwindows.

Regarding the quality of the retrieved MIPAS O_3, for daytime it has an average vertical resolution of 3-4 km below 70 km, 6-8 km at 70–80 km, 8-10 km at 80–90 km and 5–7 km at the secondary maximum (90–100 km). For nighttime conditions the vertical resolution is similar below 70 km, and it is better in the upper mesosphere and lower thermosphere. It is 4-6 km at 70–100 km (except a narrow region near 80 km where it is coarser), 4–5 km at the secondary maximum, and 6–8 km at 100–105 km. We recommend to use MIPAS O_3 only when the absolute value of the diagonal (or the mean diagonal when averaging) of the averaging kernel is larger than 0.03.

The ozone noise error for daytime is typically smaller than 2% below 50 km, 2–10% between 50 and 70 km, 10-20% at 70-90 km and ∼30% above 95 km. For nighttime, the noise errors are very similar below around 70 km but significantly smaller above, being 10-20% at 75-95 km, 20-30% at 95-100 km and larger than 30% above 100 km.

The major O_3 parameter errors are the spectroscopic data uncertainties below 50 km (10-12%) and the non-LTE and temperature errors above about 70 km. The validation analysis points to differences versus other datasets that are well within the estimated systematic uncertainties.

The non-LTE error (including the uncertainty of atomic oxygen at nighttime) is significant only above ~85 km with values of 15–20%. The temperature error varies from ~3% near 80 km to 15-20% near 100 km. Between 50 and 70 km, the pointing and the spectroscopic errors are the dominant uncertainties.

The ozone of this version shows, compared with the previous V4O_O3_m02 version (V4O_502 in some papers), an increase of 2-3% (0.2-0.5 ppmv) below around 40 km (except in the polar winter where it is smaller); a decrease of ~5-10% (~0.4-0.5 ppmv) between 40 and 50 km (due to the use of MWs of channel A only); and an increase of about 2-5% (0.1-0.2 ppmv) at 50-80 km. In the upper mesosphere, there is a general decrease of ~0.5-1 ppmv at nighttime, principally caused by neglecting the removal of $O_3(v_3)$ by chemical reaction with atomic oxygen. Above around 95 km, the O_3 in the new version is larger in about 5-10% due to the use of the larger atomic oxygen from the WACCM model.

The validation performed in comparisons with SABER, GOMOS, MLS, SMILES and ACE-FTS, shows that MIPAS O_3 has an accuracy better than 5% at and below 50 km, with a positive bias of a few percent. In that region, MIPAS systematic errors, mainly caused by the O_3 air-broadened half-widths of the v_2 band, seem to be overestimated. In the 50-75 km region MIPAS O_3 has a positive bias of approximately 10%, which is possibly caused in part by O_3 spectroscopic errors in the 10 μm region. Between 75 and 90 km, MIPAS nighttime O_3 is in agreement with other instruments by 10%. At daytime, in this region, because of the low O_3 values, the error can be ~10-20%. Above 90 km, MIPAS O_3 at daytime is in agreement with other instruments by 10%. At nighttime, however, it shows a positive bias increasing from 10% at 90 km to 20% at 95-100 km, which is attributed to the large abundances of atomic oxygen of the WACCM model.

The systematically larger O_3 measured by SABER below 50 km when compared with all instruments considered here, including MIPAS, which in this region uses the v_2 band near 14.8 μm but not the 10 μm bands used by SABER, suggests that there might be a problem in the spectroscopic data of the O_3 10 μm bands (or another unknown problem).

The global latitude coverage together with measurements at two fixed local times makes MIPAS O_3 very useful for studying the seasonal changes and partially its diurnal variation, globally in both hemispheres. The major features are summarised here. The latitudinal/seasonal distribution of daytime O_3 in the secondary maximum, near 90-95 km, shows maxima near the polar winters where the SZA is rather large and losses by photo-dissociation smaller. Near the tropics it exhibits a minimum which is attributed to tidal effects (see, e.g., Marsh et al., 2002; Dikty et al., 2010).

MIPAS O_3 data also shows the typical tertiary maximum, taking place around 60-75 km in the winter seasons at latitudes polewards of 60-70°. Its extension and magnitude are larger in the middle of the winters, and exhibit a hemispheric asymmetry with larger values in the NH. Furthermore, it has larger values during nighttime when it is usually shifted equatorwards. These features are in concordance with the results reported by Smith et al. (2017).

Note that O_3 is higher in these regions in the late fall to early winter (November-December in the NH and May-June in the SH), similar to the results reported by Smith et al. (2014). These investigators have shown that this O_3 enhancement is caused

by the relatively weak meridional circulation at those times/regions which leads to low temperatures and low H concentrations, both favouring the production of O_3.

The ozone nighttime secondary maximum presents the largest values in the early polar winters, decreases as the season progresses and recovers near the end of the winter. This is in concordance with the results reported by Smith et al. (2014).

5 Thus, during solstice, the O_3 nighttime secondary maximum shows a latitudinal gradient growing from summer to winter. During equinox, the nighttime secondary maximum exhibits an apparent signature of the diurnal migrating tide, reaching the highest vmrs (up to about 20 ppmv) at the equator near 95 km.

MIPAS O_3 upper mesospheric data also exhibit the effects of the semi-annual oscillation (SAO) in the tropics and mid-latitudes.

10 The tropical daytime O_3 at 90 km shows the lowest concentrations close to the solar cycle minimum in 2009/2010; in concordance with model simulations (Marsh et al., 2007) and explained by decreased odd oxygen production via O_2 photolysis at low solar activity conditions. At 70 km, however, one observes an opposite effect, with a tendency for ozone decreases towards 2012.

Observational evidence for a negative solar ozone response near 70 km has been provided by the Solar Mesosphere Explorer

15 (Keating et al., 1987). MIPAS data suggest, however, more of a long-term decline than a solar cycle variation, although a clear attribution is not possible due to the relatively short observation period of MIPAS.

Acknowledgements. The IAA team was supported by the Spanish MICINN under project ESP2014-54362-P and EC FEDER funds. The IAA and IMK teams were partially supported by ESA O_3-CCI and MesosphEO projects. MGC was financially supported by MINECO through its 'Ramón y Cajal' subprogram. Funding for the Atmospheric Chemistry Experiment comes primarily from the Canadian Space Agency.

20 Work at the Jet Propulsion Laboratory was performed under contract with the National Aeronautics and Space Administration.

References

Bernath, P. F.: The Atmospheric Chemistry Experiment (ACE), J. Quant. Spectrosc. Radiat. Transf., 186, 3–16, doi:10.1016/j.jqsrt.2016.04.006, 2017.

Bertaux, J. L., Kyrölä, E., Fussen, D., Hauchecorne, A., Dalaudier, F., Sofieva, V., Tamminen, J., Vanhellemont, F., Fanton D'Andon, O., Barrot, G., Mangin, A., Blanot, L., Lebrun, J. C., Pérot, K., Fehr, T., Saavedra, L., Leppelmeier, G. W., and Fraisse, R.: Global ozone monitoring by occultation of stars: an overview of GOMOS measurements on ENVISAT, Atmospheric Chemistry & Physics, 10, 12 091–12 148, doi:10.5194/acp-10-12091-2010, 2010.

Boone, C. D., Walker, K. A., , and Bernath, P. F.: Version 3 retrievals for the Atmospheric Chemistry Experiment Fourier Transform Spectrometer (ACE–FTS), in: The Atmospheric Chemistry Experiment ACE at 10: A Solar Occultation Anthology, edited by Bernath, P. F., pp. 103–127, A. Deepak Publishing, Hampton, Virginia, U.S.A., 2013.

Brasseur, G. and Solomon, S.: Aeronomy of the Middle Atmosphere–Chemistry and Physics of the Stratosphere and Mesosphere, Atmospheric and Oceanographic Sciences Library 32, Springer, P. O. Box 17, 3300 AA Dordrecht, The Netherlands, third edn., 2005.

Burkholder, J., Abbatt, J., Huie, R., Kolb, C. E., Orkin, V., Wine, P., Sander, S., Barker, J. R., Kurylo, M., and Wilmouth, D. M.: Chemical Kinetics and Photochemical Data for Use in Atmospheric Studies, Jet Propulsion Laboratory, Evaluation Number 18, 2015.

De Laurentis, M.: Planning of MIPAS new special modes January 2005 Campaign, Tech. rep., ESA Technical Note, ENVI-SPPA-EOPG-TN-05-0002, 2005.

Dikty, S., Schmidt, H., Weber, M., von Savigny, C., and Mlynczak, M. G.: Daytime ozone and temperature variations in the mesosphere: a comparison between SABER observations and HAMMONIA model, Atmospheric Chemistry and Physics, 10, 8331–8339, 2010.

Fischer, H., Birk, M., Blom, C., Carli, B., Carlotti, M., von Clarmann, T., Delbouille, L., Dudhia, A., Ehhalt, D., Endemann, M., Flaud, J. M., Gessner, R., Kleinert, A., Koopmann, R., Langen, J., López-Puertas, M., Mosner, P., Nett, H., Oelhaf, H., Perron, G., Remedios, J., Ridolfi, M., Stiller, G., and Zander, R.: MIPAS: an instrument for atmospheric and climate research, Atmos. Chem. Phys., 8, 2151–2188, 2008.

Funke, B., López-Puertas, M., Stiller, G. P., von Clarmann, T., and Höpfner, M.: A new non–LTE Retrieval Method for Atmospheric Parameters From MIPAS–ENVISAT Emission Spectra, Adv. Space Res., 27, 1099–1104, doi:10.1016/S0273-1177(01)00169-7, 2001.

Funke, B., López-Puertas, M., García-Comas, M., Kaufmann, M., Höpfner, M., and Stiller, G. P.: GRANADA: a Generic RAdiative traNsfer AnD non-LTE population Algorithm, J. Quant. Spectrosc. Radiat. Transfer, 113, 1771–1817, doi:10.1016/j.jqsrt.2012.05.001, 2012.

Garcia, R. R., Dunkerton, T. J., Lieberman, R. S., and Vincent, R. A.: Climatology of the semiannual oscillation of the tropical middle atmosphere, J. Geophys. Res., 102, 26 019 – 26 032, doi:10.1029/97JD00207, 1997.

Garcia, R. R., López-Puertas, M., Funke, B., Marsh, D. R., Kinnison, D. E., Smith, A. K., and González-Galindo, F.: On the distribution of CO_2 and CO in the mesosphere and lower thermosphere, J. Geophys. Res., 119, 5700–5718, doi:10.1002/2013JD021208, 2014.

García-Comas, M., López-Puertas, M., Marshall, B., Wintersteiner, P. P., Funke, B., Bermejo-Pantaléon, D., Mertens, C. J., Remsberg, E. E., Gordley, L. L., Mlynczak, M., and Russell, J.: Errors in SABER kinetic temperature caused by non-LTE model parameters, J. Geophys. Res., 113, D24106, doi:10.1029/2008JD010105, 2008.

García-Comas, M., Funke, B., López-Puertas, M., Bermejo-Pantaleón, D., Glatthor, N., Clarmann, T. v., Stiller, G. P., Grabowski, U., Boone, C. D., French, W. J., Leblanc, T., López-González, M. J., and Schwartz, M.: On the Quality of MIPAS Kinetic Temperature in the Middle Atmosphere, Atmos. Chem. Phys., 12, 6009–6039, doi:10.5194/acp-12-6009-2012, 2012.

García-Comas, M., Funke, B., Gardini, A., López-Puertas, M., Jurado-Navarro, A., von Clarmann, T., Stiller, G., Kiefer, M., Boone, C. D., Leblanc, T., Marshall, B. T., Schwartz, M. J., and Sheese, P. E.: MIPAS temperature from the stratosphere to the lower thermosphere: Comparison of vM21 with ACE-FTS, MLS, OSIRIS, SABER, SOFIE and lidar measurements, Atmospheric Measurement Techniques, 7, 3633–3651, doi:10.5194/amt-7-3633-2014, 2014.

Gil-López, S., López-Puertas, M., Kaufmann, M., Funke, B., García-Comas, M., Koukouli, M. E., Glatthor, N., Grabowski, U., Höpfner, M., Stiller, G. P., and von Clarmann, T.: Retrieval of stratospheric and mesospheric O_3 from high resolution MIPAS spectra at 15 and 10 μm, Adv. Space Res., 36, 943–951, doi:10.1016/j.asr.2005.05.123, 2005.

Glatthor, N., von Clarmann, T., Fischer, H., Funke, B., Gil-López, S., Grabowski, U., Höpfner, M., Kellmann, S., Linden, A., López-Puertas, M., Mengistu Tsidu, G., Milz, M., Steck, T., Stiller, G. P., and Wang, D.-Y.: Retrieval of stratospheric ozone profiles from MIPAS/ENVISAT limb emission spectra: a sensitivity study, Atmos. Chem. Phys., 6, 2767–2781, 2006.

Gordon, I. E., Rothman, L. S., Hill, C., Kochanov, R. V., Tan, Y., Bernath, P. F., Birk, M., Boudon, V., Campargue, A., Chance, K. V., Drouin, B. J., Flaud, J. M., Gamache, R. R., Hodges, J. T., Jacquemart, D., Perevalov, V. I., Perrin, A., Shine, K. P., Smith, M. A. H., Tennyson, J., Toon, G. C., Tran, H., Tyuterev, V. G., Barbe, A., Császár, A. G., Devi, V. M., Furtenbacher, T., Harrison, J. J., Hartmann, J. M., Jolly, A., Johnson, T. J., Karman, T., Kleiner, I., Kyuberis, A. A., Loos, J., Lyulin, O. M., Massie, S. T., Mikhailenko, S. N., Moazzen-Ahmadi, N., Müller, H. S. P., Naumenko, O. V., Nikitin, A. V., Polyansky, O. L., Rey, M., Rotger, M., Sharpe, S. W., Sung, K., Starikova, E., Tashkun,

S. A., Auwera, J. V., Wagner, G., Wilzewski, J., Wcisło, P., Yu, S., and Zak, E. J.: The HITRAN2016 molecular spectroscopic database, Satellite Remote Sensing and Spectroscopy: Joint ACE-Odin Meeting, October 2015, 203, 3–69, 2017.

Imai, K., Fujiwara, M., Inai, Y., Manago, N., Suzuki, M., Sano, T., Mitsuda, C., Naito, Y., Hasebe, F., Koide, T., and Shiotani, M.: Comparison of ozone profiles between Superconducting Submillimeter-Wave Limb-Emission Sounder and worldwide ozonesonde measurements, J. Geophys. Res., 118, 12,755–12,765, doi:10.1002/2013JD021094, 2013a.

Imai, K., Manago, N., Mitsuda, C., Naito, Y., Nishimoto, E., Sakazaki, T., Fujiwara, M., Froidevaux, L., von Clarmann, T., Stiller, G. P., Murtagh, D. P., Rong, P.-p., Mlynczak, M. G., Walker, K. A., Kinnison, D. E., Akiyoshi, H., Nakamura, T., Miyasaka, T., Nishibori, T., Mizobuchi, S., Kikuchi, K.-i., Ozeki, H., Takahashi, C., Hayashi, H., Sano, T., Suzuki, M., Takayanagi, M., and Shiotani, M.: Validation of ozone data from the Superconducting Submillimeter-Wave Limb-Emission Sounder (SMILES), J. Geophys. Res., 118, 5750–5769, 2013b.

Jurado-Navarro, A. A., López-Puertas, M., Funke, B., Garcia-Comas, M., Gardini, A., González-Galindo, F., Stiller, G. P., Clarmann, T. V., Grabowski, U., and Linden, A.: Global distributions of CO2 volume mixing ratio in the middle and upper atmosphere from daytime MIPAS high-resolution spectra, Atmospheric Measurement Techniques, 9, 6081–6100, doi:10.5194/amt-9-6081-2016, 2016.

Kaufmann, M., Gusev, O. A., Grossmann, K. U., Martín-Torres, F. J., Marsh, D. R., and Kutepov, A. A.: Satellite observations of daytime and nighttime ozone in the mesosphere and lower thermosphere, J. Geophys. Res., 108, 4399, doi:10.1029/2002JD003186, 2003.

Keating, G. M., Pitts, M. C., Brasseur, G., and De Rudder, A.: Response of middle atmosphere to short-term solar ultraviolet variations: 1. Observations, J. Geophys. Res., 92, 889–902, doi:10.1029/JD092iD01p00889, 1987.

Kikuchi, K.-I., Nishibori, T., Ochiai, S., Ozeki, H., Irimajiri, Y., Kasai, Y., Koike, M., Manabe, T., Mizukoshi, K., Murayama, Y., Naga-hama, T., Sano, T., Sato, R., Seta, M., Takahashi, C., Takayanagi, M., Masuko, H., Inatani, J., Suzuki, M., and Shiotani, M.: Overview and early results of the Superconducting Submillimeter-Wave Limb-Emission Sounder (SMILES), J. Geophys. Res., 115, D23 306, doi:10.1029/2010JD014379, 2010.

Kyrölä, E., Tamminen, J., Sofieva, V., Bertaux, J.-L., Hauchecorne, A., Dalaudier, F., Fussen, D., Vanhellemont, F., Fanton d'Andon, O., Barrot, G., Guirlet, M., Fehr, T., and Saavedra de Miguel, L.: GOMOS O3, NO2, and NO3 observations in 2002–2008, Atmospheric Chemistry and Physics, 10, 7723–7738, 2010.

Kyrölä, E., Tamminen, J., Sofieva, V., Bertaux, J. L., Hauchecorne, A., Dalaudier, F., Fussen, D., Vanhellemont, F., Fanton D'Andon, O., Barrot, G., Guirlet, M., Mangin, A., Blanot, L., Fehr, T., Saavedra de Miguel, L., and Fraisse, R.: Retrieval of atmospheric parameters from GOMOS data, Atmospheric Chemistry & Physics, 10, 11 881–11 903, doi:10.5194/acp-10-11881-2010, 2010.

Livesey, N. J., Read, W. G., Wagner, P. A., Froidevaux, L., Lambert, A., Manney, G. L., Millán-Valle, L. F., Pumphrey, H. C., Santee, M. L., Schwartz, M. J., Wang, S., Fuller, R. A., Jarnot, R. F., Knosp, B. W., and Martinez, E.: Version 4.2x Level 2 data quality and description document, Tech. Rep. JPL D-33509 Rev. C, Jet Propulsion Lab, 2017.

López-Puertas, M. and Taylor, F. W.: Non-LTE radiative transfer in the Atmosphere, World Scientific Pub., Singapore, 2001.

Marsh, D. R., Skinner, W. R., Marshall, A. R., Hays, P. B., Ortland, D. A., and Yee, J.-H.: High Resolution Doppler Imager observations of ozone in the mesosphere and lower thermosphere, J. Geophys. Res., 107, 4390, doi:10.1029/2001JD001505, 2002.

Marsh, D. R., Garcia, R. R., Kinnison, D. E., Boville, B. A., Sassi, F., Solomon, S. C., and Matthes, K.: Modeling the whole atmosphere response to solar cycle changes in radiative and geomagnetic forcing, J. Geophys. Res., 112, D23306, doi:10.1029/2006JD008306, 2007.

Martin-Torres, F. J.: Emisiones Infrarrojas del Ozono en la Atmósfera de la Tierra, Ph.D. thesis, Univ. of Granada, Granada, 1999.

Menard, J., Doyennette, L., and Menard-Bourcin, F.: Vibrational relaxation of ozone in O_3-O_2 and O_3-N_2 gas mixtures from infrared double-resonance measurements in the 200-300 K temperature range, J. Chem. Phys., 96, 5773, 1992.

Mitsuda, C., Suzuki, M., Iwata, Y., Manago, N., Naito, Y., Takahashi, C., Imai, K., Nishimoto, E., Hayashi, H., Shiotani, M., Sano, T., Takayanagi, M., and Taniguchi, H.: Current status of level 2 product of Superconducting Submillimeter-Wave Limb-Emission Sounder (SMILES), in: Sensors, Systems, and Next-Generation Satellites XV edited by Roland Meynart, Steven P. Neeck, Haruhisa Shimoda, edited by Meynart, R., Neeck, S. P., and Shimoda, H., vol. 8176, p. 6, SPIE, doi:10.1117/12.898135, 2011.

Mlynczak, M. G., Hunt, L. A., Mast, J. C., Thomas Marshall, B., Russell, J. M., Smith, A. K., Siskind, D. E., Yee, J.-H., Mertens, C. J., Javier Martin-Torres, F., Earl Thompson, R., Drob, D. P., and Gordley, L. L.: Atomic oxygen in the mesosphere and lower thermosphere derived from SABER: Algorithm theoretical basis and measurement uncertainty, J. Geophys. Res., 118, 5724–5735, doi:10.1002/jgrd.50401, 2013.

Moreira, L., Hocke, K., and Kämpfer, N.: Comparison of ozone profiles and influences from the tertiary ozone maximum in the night-to-day ratio above Switzerland, ACP, 17, 10 259–10 268, 2017.

Oelhaf, H.: MIPAS Mission Plan, ESA Technical Note ENVI-SPPA-EOPG-TN-07-0073, 2008.

Parrish, A., Boyd, I. S., Nedoluha, G. E., Bhartia, P. K., Frith, S. M., Kramarova, N. A., Connor, B. J., Bodeker, G. E., Froidevaux, L., Shiotani, M., and Sakazaki, T.: Diurnal variations of stratospheric ozone measured by ground-based microwave remote sensing at the Mauna Loa NDACC site: measurement validation and GEOSCCM model comparison, ACP, 14, 7255–7272, 2014.

Picone, J., Hedin, A., Drob, D., and Aikin, A.: NRLMSISE-00 empirical model of the atmosphere: Statistical comparisons and scientific issues, J. Geophys. Res., 107, 1468, doi:10.1029/2002JA009 430, 2002.

Raspollini, P., Carli, B., Ceccherini, S., Forzieri, G., Sgheri, L., Ridolfi, M., Carlotti, M., Papandrea, E., Arnone, E., Dinelli, B. M., Castelli, E., Remedios, J., Sembhi, H., Dudhia, A., Lopez-Puertas, M., Funke, B., Flaud, J.-M., von Clarmann, T., Hoepfner, M., Oelhaf, H.,

5   Fischer, H., Kiefer, M., Kleinert, A., Chipperfield, M., .Perron, G., Aubertin, G., Birk, M., Wagner, G., Gessner, R., Mosner, P., Schmitt, M., Fehr, T., D'Alba, L., and Niro, F.: Level 2 near–real–time analysis of MIPAS measurements on ENVISAT, in: Eight years of MIPAS measurements, vol. SP-686, pp. 011–d2, ESA Publication Division, 2010.

Remsberg, E. E.: On the response of Halogen Occultation Experiment (HALOE) stratospheric ozone and temperature to the 11-year solar cycle forcing, J. Geophys. Res., 113, D22304, doi:10.1029/2008JD010189, 2008.

10 Rienecker, M. M., Suarez, M. J., Gelaro, R., Todling, R., Bacmeister, J., Liu, E., Bosilovich, M. G., Schubert, S. D., Takacs, L., Kim, G.-K., Bloom, S., Chen, J., Collins, D., Conaty, A., da Silva, A., Gu, W., Joiner, J., Koster, R. D., Lucchesi, R., Molod, A., Owens, T., Pawson, S., Pegion, P., Redder, C. R., Reichle, R., Robertson, F. R., Ruddick, A. G., Sienkiewicz, M., and Woollen, J.: MERRA: NASA's Modern-Era Retrospective Analysis for Research and Applications, J. Climate, 24, 3624–3648, doi:10.1175/jcli-d-11-00015.1, 2011.

Rong, P. P., Russell, J. M., Mlynczak, M. G., Remsberg, E. E., Marshall, B. T., Gordley, L. L., and López-Puertas, M.: Validation of

15   Thermosphere Ionosphere Mesosphere Energetics and Dynamics/Sounding of the Atmosphere using Broadband Emission Radiometry (TIMED/SABER) v1.07 ozone at 9.6 μm in altitude range 15-70 km, J. Geophys. Res., 114, D04 306, doi:10.1029/2008JD010073, 2009.

Rothman, L. S., Gordon, I. E., Barbe, A., Benner, D. C., Bernath, P. F., Birk, M., Boudon, V., Brown, L. R., Campargue, A., Champion, J., Chance, K., Coudert, L. H., Dana, V., Devi, V. M., Fally, S., Flaud, J., Gamache, R. R., Goldman, A., Jacquemart, D., Kleiner, I., Lacome, N., Lafferty, W. J., Mandin, J., Massie, S. T., Mikhailenko, S. N., Miller, C. E., Moazzen-Ahmadi, N., Naumenko, O. V., Nikitin,

20   A. V., Orphal, J., Perevalov, V. I., Perrin, A., Predoi-Cross, A., Rinsland, C. P., Rotger, M., $v_S$ime$v_c$ková, M., Smith, M. A. H., Sung, K., Tashkun, S. A., Tennyson, J., Toth, R. A., Vandaele, A. C., and Vander Auwera, J.: The HITRAN 2008 molecular spectroscopic database, J. Quant. Spectrosc. Radiat. Transfer, 110, 533–572, doi:10.1016/j.jqsrt.2009.02.013, 2009.

Russell III, J. M., Mlynczak, M. G., Gordley, L. L., Tansock, J., and Esplin, R.: An overview of the SABER experiment and preliminary calibration results, in: Optical Spectroscopic Techniques and Instrumentation for Atmospheric and Space Research III, edited by Larar,

25   A. M., vol. 3756, pp. 277–288, 1999.

Sakazaki, T., Fujiwara, M., Mitsuda, C., Imai, K., Manago, N., Naito, Y., Nakamura, T., Akiyoshi, H., Kinnison, D. E., Sano, T., Suzuki, M., and Shiotani, M.: Diurnal ozone variations in the stratosphere revealed in observations from the Superconducting Submillimeter-Wave Limb-Emission Sounder (SMILES) on board the International Space Station (ISS), Journal of Geophysical Research, 118, 2991–3006, 2013.

30 Schanz, A., Hocke, K., and Kämpfer, N.: Daily ozone cycle in the stratosphere: global, regional and seasonal behaviour modelled with the Whole Atmosphere Community Climate Model, ACP, 14, 7645–7663, 2014.

Schwartz, M., Froidevaux, L., Livesey, N., and Read, W.: MLS/Aura Level 2 Ozone (O3) Mixing Ratio V004, in: Accessed October 2017, Goddard Earth Sciences Data and Information Services Center (GES DISC), doi:doi: 10.5067/AURA/MLS/DATA2017, 2015.

Sheese, P. E., Walker, K. A., Boone, C. D., Bernath, P. F., Froidevaux, L., Funke, B., Raspollini, P., and von Clarmann, T.: ACE-FTS

35   ozone, water vapour, nitrous oxide, nitric acid, and carbon monoxide profile comparisons with MIPAS and MLS, Journal of Quantitative Spectroscopy and Radiative Transfer, 186, 63 – 80, doi:10.1016/j.jqsrt.2016.06.026, 2017.

Smith, A. K., Harvey, V. L., Mlynczak, M. G., Funke, B., García-Comas, M., Hervig, M., Kaufmann, M., Kyrölä, E., López-Puertas, M., McDade, I., Randall, C. E., Russell, J. M., Sheese, P. E., Shiotani, M., Skinner, W. R., Suzuki, M., and Walker, K. A.: Satellite observations of ozone in the upper mesosphere, J. Geophys. Res., 118, 1–19, doi:10.1002/jgrd.50445, 2013.

40 Smith, A. K., López-Puertas, M., Funke, B., García-Comas, M., Mlynczak, M. G., and Holt, L. A.: Nighttime ozone variability in the high latitude winter mesosphere, J. Geophys. Res., doi:10.1002/2014JD021987, 2014.

Smith, A. K., Espy, P. J., Lopez-Puertas, M., and Tweedy, O. V.: Spatial and temporal structure of the tertiary ozone maximum in the polar winter mesosphere, J. Geophys. Res., submitted, 2017.

Sofieva, V. F., Kyrölä, E., Verronen, P. T., Seppälä, A., Tamminen, J., Marsh, D. R., Smith, A. K., Bertaux, J.-L., Hauchecorne, A., Dalaudier,

45   F., Fussen, D., Vanhellemont, F., Fanton d'Andon, O., Barrot, G., Guirlet, M., Fehr, T., and Saavedra, L.: Spatio-temporal observations of the tertiary ozone maximum, Atmospheric Chemistry and Physics, 9, 4439–4445, 2009.

Sofieva, V. F., Vira, J., Kyrölä, E., Tamminen, J., Kan, V., Dalaudier, F., Hauchecorne, A., Bertaux, J.-L., Fussen, D., Vanhellemont, F., Barrot, G., and Fanton D'Andon, O.: Retrievals from GOMOS stellar occultation measurements using characterization of modeling errors, Atmospheric Measurement Techniques, 3, 1019–1027, 2010.

50 Sofieva, V. F., Rahpoe, N., Tamminen, J., Kyrölä, E., Kalakoski, N., Weber, M., Rozanov, A., von Savigny, C., Laeng, A., von Clarmann, T., Stiller, G. P., Lossow, S., Degenstein, D., Bourassa, A., Adams, C., Roth, C., Lloyd, N., Bernath, P., Hargreaves, R. J., Urban, J., Murtagh, D., Hauchecorne, A., Dalaudier, F., van Roozendael, M., Kalb, N., and Zehner, C.: Harmonized dataset of ozone profiles from satellite limb and occultation measurements, Earth System Science Data, 5, 349–363, 2013.

Studer, S., Hocke, K., Schanz, A., Schmidt, H., and Kämpfer, N.: A climatology of the diurnal variations in stratospheric and mesospheric ozone over Bern, Switzerland, ACP, 14, 5905–5919, 2014.

Takahashi, C., Ochiai, S., and Suzuki, M.: Operational retrieval algorithms for JEM/SMILES level 2 data processing system, Satellite Remote Sensing and Spectroscopy: Joint ACE-Odin Meeting, October 2015, 111, 160–173, 2010.

5 Takahashi, C., Suzuki, M., Mitsuda, C., Ochiai, S., Manago, N., Hayashi, H., Iwata, Y., Imai, K., Sano, T., Takayanagi, M., and Shiotani, M.: Capability for ozone high-precision retrieval on JEM/SMILES observation, Advances in Space Research, 48, 1076–1085, 2011.

Tamminen, J., Kyrölä, E., Sofieva, V. F., Laine, M., Bertaux, J.-L., Hauchecorne, A., Dalaudier, F., Fussen, D., Vanhellemont, F., Fanton-D'Andon, O., Barrot, G., Mangin, A., Guirlet, M., Blanot, L., Fehr, T., Saavedra de Miguel, L., and Fraisse, R.: GOMOS data characterisation and error estimation, Atmospheric Chemistry & Physics, 10, 9505–9519, doi:10.5194/acp-10-9505-2010, 2010.

10 Tikhonov, A.: On the solution of incorrectly stated problems and method of regularization, Dokl. Akad. Nauk. SSSR, 151, 501–504, 1963.

von Clarmann, T. and Echle, G.: Selection of optimized microwindows for atmospheric spectroscopy, Appl. Opt., 37, 7661–7669, 1998.

von Clarmann, T., Glatthor, N., Grabowski, U., Höpfner, M., Kellmann, S., Kiefer, M., Linden, A., Mengistu Tsidu, G., Milz, M., Steck, T., Stiller, G. P., Wang, D. Y., Fischer, H., Funke, B., Gil-López, S., and López-Puertas, M.: Retrieval of temperature and tangent altitude pointing from limb emission spectra recorded from space by the Michelson Interferometer for Passive Atmospheric Sounding (MIPAS),

15 J. Geophys. Res., 108, 4736, doi:10.1029/2003JD003602, 2003.

von Clarmann, T., Höpfner, M., Kellmann, S., Linden, A., Chauhan, S., Grabowski, U., Funke, B., Glatthor, N., Kiefer, M., Schieferdecker, T., , and Stiller, G. P.: Retrieval of temperature H_2O, O_3, HNO_3, CH_4, N_2O and $ClONO_2$ from MIPAS reduced resolution nominal mode limb emission measurements, Atmos. Meas. Tech., 2, 159–175, 2009.

von Clarmann, T., Funke, B., López-Puertas, M., Kellmann, S., Linden, A., Stiller, G. P., Jackman, C. H., and Harvey, V. L.: The Solar Proton

20 Events in 2012 as Observed by MIPAS, Geophys. Res. Lett., 40, 1–5, doi:10.1002/grl.50119, 2013.

Waters, J. W., Froidevaux, L., Harwood, R. S., Jarnot, R. F., Pickett, H. M., Read, W. G., Siegel, P. H., Cofield, R. E., Filipiak, M. J., Flower, D. A., Holden, J. R., Lau, G. K., Livesey, N. J., Manney, G. L., Pumphrey, H. C., Santee, M. L., Wu, D. L., Cuddy, D. T., Lay, R. R., Loo, M. S., Perun, V. S., Schwartz, M. J., Stek, P. C., Thurstans, R. P., Boyles, M. A., Chandra, K. M., Chavez, M. C., Chen, G.-S., Chudasama, B. V., Dodge, R., Fuller, R. A., Girard, M. A., Jiang, J. H., Jiang, Y., Knosp, B. W., Labelle, R. C., Lam, J. C., Lee, A. K., Miller, D.,

25 Oswald, J. E., Patel, N. C., Pukala, D. M., Quintero, O., Scaff, D. M., Vansnyder, W., Tope, M. C., Wagner, P. A., and Walch, M. J.: The Earth Observing System Microwave Limb Sounder (EOS MLS) on the Aura Satellite, IEEE Transactions on Geoscience and Remote Sensing, 44, 1075–1092, doi:10.1109/TGRS.2006.873771, 2006.

West, G. A., Weston Jr., R. E., and Flynn, G. W.: Deactivation of vibrationally excited ozone by $O(^3P)$ atoms, Chem. Phys. Lett., 42, 488–493, 1976.

30 West, G. A., Weston, R. E., and Flynn, G. W.: The influence of reactant vibrational excitation on the $O(^3P)$+O_3 bimolecular reaction rate, Chem. Phys. Lett., 56, 429–433, 1978.